Cancer Letters 581 (2024) 216484

Contents lists available at ScienceDirect

Cancer Letters

journal homepage: www.elsevier.com/locate/canlet

Original Articles

MGRN1 depletion promotes intercellular adhesion in melanoma by upregulation of E-cadherin and inhibition of CDC42

S. Cerdido, M. Abrisqueta, J. Sánchez-Beltrán, A. Lambertos, M. Castejón-Griñán [1], C. Muñoz, C. Olivares, J.C. García-Borrón, C. Jiménez-Cervantes, C. Herraiz [*]

Department of Biochemistry, Molecular Biology and Immunology, School of Medicine, University of Murcia, Instituto Murciano de Investigación Biosanitaria (IMIB), 30120, Murcia, Spain

ARTICLE INFO

Keywords:
Melanoma
MGRN1
Cell adhesion
E-cadherin

ABSTRACT

Mahogunin Ring Finger 1 is an E3-ubiquitin ligase encoded by the color gene *MGRN1*. Our previous *in vitro* and *in vivo* studies demonstrated that Mgrn1 deletion in mouse melanoma cells induced cell differentiation and adhesion, and decreased cell motility and invasion on collagen I, and lung colonization in an *in vivo* model. Here, we investigated the role of MGRN1 on human melanoma cell morphology, adhesion and expression of genes/proteins involved in an EMT-like transition. We demonstrated that wild-type BRAF human melanoma cells adopted a clustering-like morphology on collagen I, with permanent MGRN1 abrogation resulting in bigger cell clusters. Enhanced intercellular adhesion was mostly mediated by induction of E-cadherin and higher co-localization with β-catenin. Transcriptional upregulation of E-cadherin likely occurred through downregulation of the ZEB1 repressor. Finally, pulldown assays showed reduced activation of CDC42 in the absence of MGRN1, which was reverted after E-cadherin silencing. Overall, these findings highlight a new MGRN1-dependent pathway regulating melanoma cell shape, motility, and invasion potential.

1. Introduction

Mahogunin Ring Finger 1 (MGRN1 or mahogunin) is a ubiquitous protein with a C3HC4 Really Interesting New Gene (RING) Finger domain, characteristic of E3-ubiquitin ligases. Mahogunin is encoded by the *MGRN1* gene lying on chromosome 16 and containing 17 exons. Alternative splicing of exons 12 and 17 yields four MGRN1 isoforms [1,2], all of which carry exon 10 coding for the RING Finger domain. In mice, a mutation in *Mgrn1* gene was known as *mahoganoid* (*md*) coat color mutation [3], due to the similar phenotypic effects to the coat color mutant mahogany (Atrn(mg)). *Md* mice displayed hyperpigmentation, which has recently been shown to be due to increased melanosomal pH and tyrosinase activity [4]. Loss of Mgrn1 in mice also caused late-onset spongiform neurodegeneration with many features of prion diseases [5], congenital heart defects and embryonic lethality [6]. This pleiotropic phenotype suggested that MGRN1 may be involved in multiple biological processes. Indeed, MGRN1 was found to: i) modulate melanocortin signaling by decreasing melanocortin 1 receptor (MC1R) and MC4R signaling to cAMP through the competition with Gαs [1], as well as inducing ubiquitination of regulatory β-arrestins in the presence of MC1R [7]; ii) regulate endo-lysosomal trafficking by interacting with and promoting ubiquitination of TSG101, an ESCRT-I component, involved in endocytosis [8]; iii) participate in mitochondrial homeostasis through the calmodulin-mediated ubiquitination of the endoplasmic reticulum E3 ligase GP78 involved in mitophagy [9] and the ubiquitination of Mitofusin 1 affecting mitochondria fusion [10], among others; iv) affect the orientation of the mitotic spindle and microtubule dynamics through ubiquitination of the cytoskeletal protein α-tubulin [11] and; v) regulate the genomic stability and the malignant phenotype of melanoma cells [12,13]. Regarding the latter, we have demonstrated that loss of expression of Mgrn1 in mouse melanoma cells induced a more differentiated phenotype with more dendricity, less motility, more adhesion to a collagen I matrix and less lung colonization potential in an *in vivo* mouse model of intravenous injection of Mgrn1-depleted melanoma cells. These results strongly suggested that Mgrn1 may affect the aggressiveness of melanoma cells. However, no similar human

* Corresponding author.
E-mail address: ceciliahs@um.es (C. Herraiz).
[1] Present address: Centro Andaluz de Biología Molecular y Medicina Regenerativa (CABIMER), Consejo Superior de Investigaciones Científicas (CSIC), Universidad de Sevilla, 41013, Sevilla, Spain.

https://doi.org/10.1016/j.canlet.2023.216484
Received 30 June 2023; Received in revised form 25 October 2023; Accepted 3 November 2023
Available online 25 November 2023
0304-3835/© 2023 The Authors. Published by Elsevier B.V. This is an open access article under the CC BY-NC license (http://creativecommons.org/licenses/by-nc/4.0/).

phenotype comparable with the *mahoganoid* has been described, and the function of MGRN1 in human melanoma cells remains unclear.

Melanoma is the deadliest form of skin cancer, with a high potential for invasion and metastatic spread [14]. Malignant transformation of melanocytes occurs through complex processes involving the acquisition of a more proliferative and invasive potential, leading to tumor dissemination and metastasis [15]. These events are promoted by accumulation of gene and protein mutations, allowing tumor cells to lose contact with surrounding keratinocytes, to proliferate aberrantly and migrate from the primary tumor. Even though melanoma is not an epithelial cancer, melanoma cells undergo a phenotype switch similar to the epithelial to mesenchymal transition (EMT) of epithelial tumors that contributes to tumor progression [16,17]. In melanoma, this EMT-like program is characterized by loss of epithelial (E)-cadherin expression [18,19]. Cadherins are transmembrane glycoproteins involved in Ca^{2+}-dependent cell-cell adhesion, being E-cadherin the best studied member. E-cadherins form adherens junctions and interconnect the cytoskeletons of adjacent cells. Remodeling of the cytoskeleton occurs through interaction of the cytoplasmic region of E-cadherin with catenins, which in turn connect with the actin cytoskeleton and regulate many cellular processes, such as tumor progression [20]. Thus, elucidating the mechanisms of regulation of E-cadherin expression is of utmost importance to develop effective therapeutic strategies to reduce cell dissemination.

In a recent study, we investigated the potential role of MGRN1 as a therapeutic melanoma biomarker [12]. Importantly, analysis of the data compiled in the GEPIA and TCGA databases revealed that *MGRN1* is significantly overexpressed in the tumor with respect to normal skin and that high MGRN1 expression is associated with shorter survival of patients. Moreover, preliminary experiments showed that persistent knockdown of MGRN1 expression led to increased dendricity by a likely MITF-independent mechanism, and increased genomic instability, as MGRN1-null cells displayed higher levels of γ-H2AX labeling and increased tail moment in an alkaline comet assay, indicative of higher abundance of DNA breaks with respect to control cells [12]. In this study, we aimed to look deeper into the effect of MGRN1 deficiency on human melanoma cell morphology and to investigate key molecules modulated by MGRN1 that could account for this phenotypic switch. Interestingly, we found that wild-type (WT)-BRAF human melanoma cells displayed a clustering-like morphology on a collagen I matrix and that MGRN1 depletion increased the area of these spherical aggregates. Furthermore, analysis of the molecular mechanism of this phenotypic switch suggested that, in WT-BRAF human melanoma cells, MGRN1 regulates intercellular aggregation by modulating E-cadherin expression and CDC42 activity. Altogether, our data further support that modulation of MGRN1 function could reduce melanoma aggressiveness.

2. Materials and methods

2.1. Antibodies and inhibitors

RNF156 (Anti-MGRN1, rabbit polyclonal, 1:4000 dilution, #11285 Proteintech), MGRN1 (rabbit polyclonal, 1:2000 dilution, LS-c752973 LSBio), Actin (rabbit, 1:10000 dilution, #A2066 Sigma-Aldrich), RAC1 (mouse monoclonal, 1:1000 dilution, 05–389 Millipore). E-cadherin (mouse monoclonal, 1:100 dilution, #14472) and CDC42 (rabbit monoclonal, 1:2000 dilution, #2466) were from Cell Signaling. TATA binding protein TBP (rabbit polyclonal, 1:3000 dilution, ab63766 Abcam), N-cadherin (rabbit monoclonal, January 2000 dilution, ab76011) and ZEB1 (rabbit monoclonal, 1:2000, ab203829) were from Abcam. SLUG (rabbit polyclonal, 1:2000, GTX128796), P120 (mouse monoclonal, 1:100, GTX11508) and ZO-1 (rabbit polyclonal, 1:100, GTX108613) were from GeneTex. GAPDH (rabbit polyclonal, 1:5000 dilution, sc-25778), β-catenin (mouse monoclonal, 1:5000 dilution, sc-7963), E-cadherin (mouse monoclonal, 1;1500 dilution, sc-8426), Connexin 43 or GJA (mouse monoclonal, 1:1000 dilution, sc-271837 and sc-59949), RAC-GAP1 (mouse monoclonal, 1;1000 dilution, sc-271110), ARH-GAP17 (mouse monoclonal, 1;1000 dilution, sc-514438) and FOXM1 (mouse monoclonal, 1:2000 dilution, sc-376471) were from Santa Cruz. Alexa Fluor 488 (mouse, 1:400, A-11017) and Alexa Fluor 568 (rabbit, 1:400, A-21069) were from Invitrogen.

Rac inhibitor III (1 μM; 553513) and Cycloheximide (10^{-4} M) were from Calbiochem. CDC42 inhibitor (2 μM and 10 μM; ML141, SML0407) was from Sigma-Aldrich.

2.2. Cell culture

HBL, DOR, MM28, BEU and C8161 human melanoma cells were kindly provided by Prof. G. Ghanem (LOCE-Institut J. Bordet, Université Libre de Bruxelles, Belgium), and were grown in DMEM enriched with 10 % fetal serum bovine (FBS), 100 U/mL penicillin and 100 μg/mL streptomycin sulfate. Cells were cultured every week until 80 % confluence.

2.3. Plasmids and transient transfection

MGRN1-S(+)-CFP construct was obtained by cloning the *MGRN1-S(+)* coding sequence into the pECFP-C1 plasmid (BD Biosciences Clontech, CA). We designed the following PCR primers to amplify *MGRN1-S(+)* cDNA from the MGRN1-HA-pcDNA3 construct [1] and cloned it into the MCS in the same reading frame as ECFP with no intervening in-frame stop codons. The primers were MGRN1-CFP_Fw (CCCAAGCTTCCGG CTCCATTCTCAGCCG) and MGRN1-CFP_Rv (GCGGAATTCTTACTCG TCTATACCAACAG). *Hind*III and *Eco*RI restriction sites (underlined) were chosen as the insertion spots. The gene was then expressed as a fusion protein to the C-terminus of ECFP.

Cells seeded on coverslips in 24-well plates were transfected with construct *MGRN1-S(+)-CFP,* using Lipofectamine 2000 (1 mg/mL) (Invitrogen #11668-019) as a transfection reagent. Lipofectamine (1 μL) and MGRN1-S(+)-CFP plasmid (150 ng/μL) were diluted in OptiMEM™ (Gibco #31985070) and incubated for 5 min at room temperature (RT). Then, Lipofectamine and plasmid solutions were mixed (1:1) for 20 min at RT. For control condition, only the mixture of Lipofectamine and OptiMEM was used. Finally, DMEM enriched with 10 % FBS was added to a final volume of 350 μL per well.

2.4. Cell morphology assay on plastic flasks and on collagen I system

For cell morphology assays on plastic flasks, cells were seeded in a 12-well plate at 30 % confluence and were imaged after 24–72 h using Nikon Eclipse Ts2 microscope. Analysis of cell morphology followed the criterion: percentage of rounded cells versus dendritic cells. On morphology collagen assays, collagen I matrices were prepared using atelopeptide fibrillar bovine dermal collagen (5005-B; PureCol, Advanced BioMatrix) at a final concentration of 1.7 mg/mL in Minimum Essential Media (MEM) and allowed to polymerize for 4 h. Collagen I matrices at this concentration has been reported to mimic the size of collagen fibers and the diameter of the pores of mouse dermis [21]. After polymerization, cells were seeded on top of collagen in medium containing 1 % or 10 % FBS. Cells were imaged after 24–48 h. Assessment of cell morphology accomplished the following criteria: percentage of cell aggregates versus single cells and percentage of rounded cells versus elongated cells. In melanoma cell lines forming cellular clusters on collagen I, ImageJ (https://imagej.nih.gov) was used to measure the area of the aggregates using the free-hand tool.

2.5. 2D migration assay

Cellular migration assay was performed using the Oris™ Universal Assembly Kit (CMAU505), following manufacturer's protocol. Cells (6.5×10^4) were seeded in a 96 well-plate with silicon cell seeding stoppers in serum reduced medium and cell attachment was permitted for 24 h.

All stoppers were then removed using the Oris Stopper Tool. Images were taken after stoppers removal (t = 0 h) and after 24 h of migration (t = 24 h). Wound closure percentage (%) was determined by measuring the wound area at both time points using Image J.

2.6. Adhesion assay on collagen I

Adherent cells were detached using a non-enzymatic cell dissociation solution and cells (10^4) were seeded on a thick layer of collagen I (1.7 mg/mL), prepared as mentioned above, in a 96-well plate in serum-free medium. After 1 h at 37 °C, cells were imaged with a bright field microscope using a 4x objective. Plates were washed once with PBS and re-imaged. Percentage of adhering cells was calculated as the number of cells remaining after washing, using the "Cell counter" tool of ImageJ.

2.7. Melanoma spheroids

Spheroids were generated using the hanging drop method, as previously described [13]. Briefly, spheroids of HBL control and MGRN1-null cells were collected and embedded in a collagen I matrix (1.7 mg/mL). After collagen polymerization, images of spheroids were taken at time point 0 and after 4 days of growing. Quantification of the increase in the area (ΔArea) was measured by Image J.

2.8. Generation of CRISPR/Cas9-Based MGRN1-KO cells

Target sequences for CRISPR-RNA from Dharmacon are specified on Supplemental Table 1. Efficiencies and potential off-targets were determined using the Breaking-Cas web server (https://bioinfogp.cnb.csic.es/tools/breakingcas/) [22]. Cells were transfected with 0.5 μg of the CRISPR plasmid (pSpCas9(sgRNA2, sgRNA3 or sgRNA4)) and 1 mg/mL Lipofectamine 2000. For negative control cells, the empty plasmid (pSpCas9) was transfected. After incubation for 72 h at 37 °C, puromycin-resistant clonal cells were selected. Confirmation and selection of positive clones was performed by automated sequencing after PCR amplification of a 500-pb fragment on exon 1 using genomic DNA as template and by Western blot detection.

2.9. RNAi transfection

Human melanoma cells were seeded in the adequate plate according to the experiment and the following day, cells were transfected with a stoichiometric mixture of human MGRN1 siRNA oligonucleotides siGENOME for silencing MGRN1 or with human CDH1 siRNA oligonucleotides for silencing E-cadherin, at a final concentration of 30 nM, using Opti-MEM (Invitrogen) and 5 μL/well of DharmaFECT 4 Transfection Reagent from Dharmacon (Lafayette, CO, USA). Non-targeting siRNA was used as control. Forty-eight or 72 h later, cells were used for the desired experiment. siRNA sequences are specified on Supplemental Table 2.

2.10. RNA extraction

RNA extraction of HBL MGRN1-KO melanoma cells was isolated using RNeasy® Mini kit (QIAGEN) and following manufacturer's instructions.

2.11. cDNA synthesis

One microgram of RNA was reverse-transcribed to cDNA using the commercial kit SuperScriptTM First-Strand Synthesis System for RT-PCR (Invitrogen) and following manufacturer's instructions.

2.12. Quantitative RT-PCR

RT-PCR was performed using the Power SYBR Green PCR Master Mix (Applied Biosystem) on ABI 7500 Fast Real Time PCR System. β-actin was used as an endogenous normalizer. See Supplemental Table 3 for primers' sequences.

2.13. Sequencing of NF1

The NF1 genotype was determined by sequencing of the PCR-amplified products using Sanger sequencing (Molecular Biology Platform, University of Murcia). Amplified fragment of NF1 corresponds to the RAS-GAP related domain (GDR), which comprises amino acids 1235–1451 and is encoded by exons 27–33 (https://www.uniprot.org/). Sequence was compared with NF1-202 sequence obtained from Ensembl database (https://www.ensembl.org/index.html). Primers used for sequencing are described in Supplemental Table 4.

2.14. Gene expression and enrichment analyses

Total RNA from MGRN1-KO melanoma cells (clone 4.9) and control cells was isolated and purified with RNeasy® Mini kit (QIAGEN) as described above. Complementary DNA synthesis, DNA library construction, quality control evaluations and transcriptomic analysis were performed by Novogene Co., Ltd, using Illumina sequence method (Illumina NovaSeq 6000 platform). Raw data counts normalization and processing was accomplished using RStudio package DESeq2 [23].

Gene set enrichment analysis was performed using GSEA_4.3.2. software (http://www.broadinstitute.org/gsea/index.jsp), collapsing a data set containing 32,583 features into the Molecular Signature Database human gene sets collection (MSigDB v.2022.1) [24,25]. Gene sets enriched in MGRN1-KO cells versus control cells were considered significant according to p value < 0.05 and false discovery rate (FDR) < 0.25.

A heatmap of a custom set of genes involved in cell adhesion was generated using Heatmapper software (http://www.heatmapper.ca/).

2.15. Immunoblotting

Cells were lysed using Lysis Buffer (50 mM Tris-HCl pH 7.5, 1 mM EDTA, 1 % Igepal) or RIPA Buffer (50 mM Tris-HCl pH 8, 150 mM NaCl, 0.5 % Sodium deoxycholate, 0.1 % SDS, 1 % Triton X-100) supplemented with 0.1 mM phenylmethylsulfonyl fluoride (PMSF), 10 mM iodoacetamide (IAA), 10 mM N-ethylmaleimide (NEM) and phosphatase inhibitors (200 mM imidazole, 100 mM NaF, 100 mM Na_3VO_4 and 1 M β-Glycerol phosphate). Lysates were collected by gentle shaking and centrifuged for 30 min at 15,000 g at 4 °C. Supernatants were prepared with 4X Loading Sample Buffer (250 mM Tris pH 6.8, 8 % SDS, 20 % glycerol, 0.08 % bromophenol blue and 3.2 M β-mercaptoethanol). Electrophoresis of the samples was performed on polyacrylamide gels in the presence of SDS (sodium dodecyl sulfate). Cell lysates were resolved by SDS-polyacrylamide (PAGE) and transferred onto a PVDF membrane (Immobilon-P). The ECL Plus detection System (GE Healthcare) with HRP-conjugated secondary antibodies (GE Healthcare) was used for detection. Bands' intensities were quantified using ImageJ and data were always normalized to a loading control.

2.16. Protein half-life

Cells were seeded on a 12 well-plate at 70–80 % confluence and treated with 10^{-4} M of cycloheximide (Calbiochem) for 30 min. Lysates were collected at different times using Lysis Buffer and prepared with 4X Loading Sample Buffer. Samples were boiled for 5 min and resolved by SDS-PAGE.

2.17. Cell fractioning using CSK buffer

Cells (10^6) were collected with trypsin, washed with PBS 1X and resuspended with 200 μl of Cytoskeletal Buffer (CSK Buffer: 10 mM

PIPES pH 6.8, 100 mM NaCl, 300 mM sucrose, 3 mM $MgCl_2$, 1 mM EGTA, 50 mM NaF, 0.1 mM Na_3VO_4 and 0.1 % Triton X-100) supplemented by protease inhibitors. Samples were briefly vortexed, incubated on ice for 10 min and centrifugated at low speed for 5 min. The supernatant constituted the soluble fraction (Cytosol + Nucleosol fraction of proteins) and the pellet the insoluble fraction (Chromatin-bound proteins). Insoluble fraction was washed twice with CSK buffer and SDS-PAGE loading buffer was added for analyzing chromatin-bound/unbound proteins by SDS-PAGE.

2.18. Confocal fluorescent microscopy

For membrane-associated E-cadherin and nuclear β-catenin expression, cells were fixed in 4 % *p*-formaldehyde, permeabilized with 0.3 % Triton-X 100 (v/v) and blocked with 4 % BSA. Cells were labeled with anti-E-cadherin monoclonal antibody (Cell Signaling) or with β-catenin monoclonal antibody (Santa Cruz), followed by an Alexa 488- conjugated secondary antibody. F-actin was stained using Phalloidin eFluor-570 or Phalloidin eFluor-660 (eBioscience, Paisley, UK) and DNA was stained using DAPI. Samples were imaged with a SP8 Leica laser scanning confocal microscope and software (Leica Microsystems GmbH, Wetzlar, Germany) with HCXPL APO CS 63x objective lenses. Membrane-associated E-cadherin fluorescence signal was quantified by calculating the pixel intensity in single cell cytoplasm relative to the cytoplasm area using F-actin. Nuclear β-catenin fluorescence signal was quantified by calculating the pixel intensity in single cells relative to the nuclei area using DAPI.

For E-cadherin/β-catenin colocalization, cells were fixed in 4 % *p*-formaldehyde, permeabilized with 0.1 % saponin and blocked with 4 % BSA. Cells were labeled with anti-E-cadherin monoclonal antibody (Cell Signaling) and β-catenin monoclonal antibody (Santa Cruz), followed by an Alexa 488- and Alexa-569 conjugated secondary antibodies, respectively. F-actin was stained using Phalloidin eFluor-660 (eBioscience, Paisley, UK) and DNA was stained using DAPI. Samples were imaged with a SP8 Leica laser scanning confocal microscope and software (Leica Microsystems GmbH, Wetzlar, Germany) with HCXPL APO CS 63x objective lenses.

Colocalization quantifications were performed using the Coloc2 tool in ImageJ, overlapping two channels and calculating the Manders' overlap coefficient.

For rescue assays, staining was performed as above, using propidium iodide (red) to stain nuclei. Non-transfected and transfected cells (in blue) of clone 2.1 were measured.

2.19. RAC1-GTP and CDC42-GTP pulldown assays

Cells (1.5×10^6) were seeded in a P100 plate and serum deprived the next day. After 12 h without serum, cells were lysed in Magnesium-containing lysis buffer (MLB) (25 mM HEPES pH 7.5, 150 mM NaCl, 1 % Igepal CA-630, 10 % Glycerol, 25 mM NaF, 10 mM $MgCl_2$, 1 mM EDTA, 1 mM sodium Na_3VO_4 and 10 μg/μL leupeptin). Protein lysates were centrifugated at 17,000 g 4 °C for 30 min and a small proportion was mixed with LDS loading buffer for determination of total RAC1 and CDC42 levels. The remaining protein lysate was incubated with Glutathione S-transferase (GST)-conjugated PAK-1 agarose beads for 1 h (to detect RAC1 and CDC42 activity). Beads were collected by centrifugation, washed several times with MLB and resuspended with LDS 2X loading buffer. Samples were boiled for 5 min and supernatants were collected and resolved by SDS-PAGE.

2.20. Time-lapse microscopy

Cells (10^5) were seeded on top of a collagen I matrix in a glass bottom 24-well plate. Multi-site bright-field images were taken every 10 min for 24 h in a humidified chamber at 37 °C and 5 % CO_2, using a SP8 Leica laser scanning confocal microscope with PL APO 10x objective lenses.

2.21. Statistical analysis

All analyses were carried out using GraphPad Prism. For comparisons of two groups, normality test was performed, and Unpaired two-tailed Student's *t*-test was applied when variance among groups was not statistically different. For non-normal distribution, U of Mann Whitney test was performed. When comparing more than two groups, normality test was performed and One-way Anova with Dunnett's post-test was applied when variance among groups was not statistically different. When variance was different, Kruskal-Wallis test with Dunn's post-test was performed. Results are expressed as mean ± SEM or as median and indicated in each figure. *p* values of less than 0.05 were considered statistically significant. * indicates $p < 0.05$, **, $p < 0.01$, ***, $p < 0.001$ and ****, $p < 0.0001$.

3. Results

3.1. Repression of MGRN1 resulted in increased intercellular adhesion on collagen I in WT-BRAF human melanoma cells

We have previously shown that Mgrn1 ablation in mouse melanocytes and melanoma cells led to a more differentiated phenotype, with more dendritic cells, higher adhesion to collagen matrices and less motility. In mouse melanoma cells, knockdown of Mgrn1 also decreased lung colonization ability, suggesting that Mgrn1 levels affected their invasive potential [13].

The effects of MGRN1 knockdown on human melanoma cells are largely unknown. Accordingly, we investigated whether deletion of MGRN1 in a panel of human melanoma cells would lead to a phenotype comparable to Mgrn1-KO mouse melanoma cells. We tested five human melanoma cell lines with different genetic backgrounds for *NRAS*, *BRAF* and *MC1R*. *NRAS and BRAF* are the most prevalent significantly mutated genes in cutaneous melanoma [26,27], with gain-of-function mutations in *BRAF* and *NRAS* occurring in 50 % and 15–20 % of melanomas, respectively [28,29]. MC1R is an important susceptibility gene predisposing to cutaneous melanoma and a major genetic determinant of cutaneous pigmentation [30], as well as a MGRN1-interacting partner [1,7]. HBL and MM28 melanoma cells were WT for these genes, DOR cells harbored NRAS mutation Q61R in heterozygosis with the WT allele, and BEU and C8161 cells were homozygous for the BRAF mutation V600E, thus comprising a good representation of melanoma cell lines (Supplemental Fig. 1A). All cell lines were WT for *NF1*. Pellets of the different melanoma cells were collected to assess melanin content and revealed that NRAS- and BRAF-mutated cell lines were amelanotic (DOR, BEU and C8161), whereas the cell lines WT for these genes, HBL and MM28, were significantly pigmented (Supplemental Fig. 1A). Levels of MGRN1 expression were studied by Western blot. We found comparable MGRN1 expression for HBL, MM28 and DOR cell lines, and lower levels for BEU and C8161 cells (Supplemental Fig. 1B).

We investigated the effect of MGRN1 repression on cell morphology using $2^{1/2}$ fibrillar collagen I systems to recapitulate melanoma extracellular matrix *in vitro*, since type I collagen is the main component of the dermis. MGRN1 expression was decreased by transfection with a mixture of four siRNA oligonucleotides targeting all MGRN1 isoforms for 72 h (Fig. 1A, top panels). MGRN1-depleted melanoma cells were seeded on a thick layer of atelopeptide bovine dermal collagen I, and cell morphology was assessed in a tissue-like environment. Interestingly, WT-BRAF melanoma cells (HBL, MM28 and DOR cells) grew in groups as spherical cellular aggregates, comprising approximately 50 % of the cell population, whereas the other 50 % of the cells grew as individual rounded/amoeboid-like cells, indicating that these cell lines might express high levels of cell-cell adhesion molecules (Fig. 1A, middle panels). Among these WT-BRAF melanoma cell lines, the biggest cell aggregates were found in HBL cells followed by MM28, whereas DOR cells displayed the smallest spheres. Repression of MGRN1 in these WT-BRAF melanoma cell lines increased the size of cell clusters and the

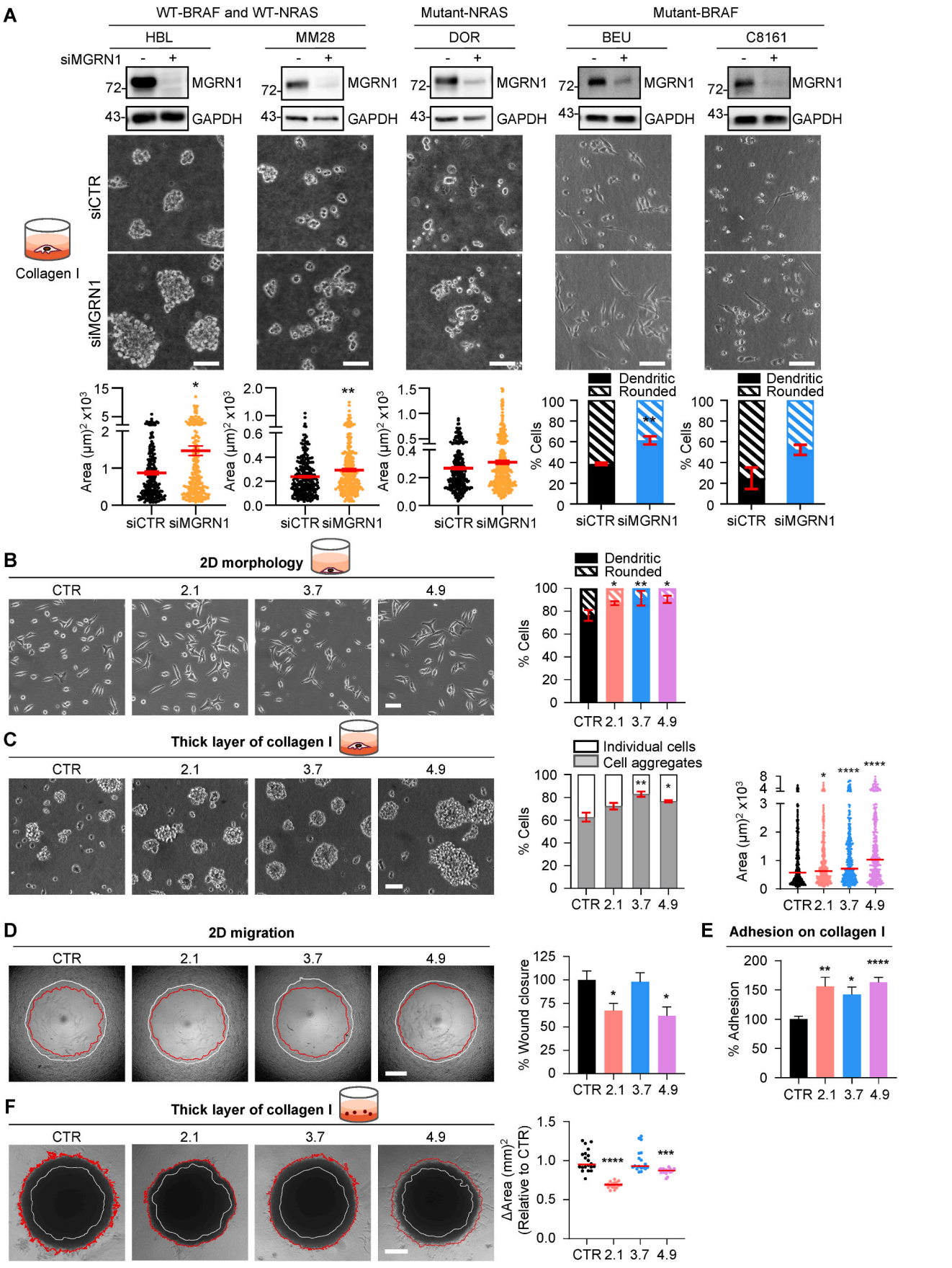

(caption on next page)

Fig. 1. Phenotypic switch upon MGRN1 deletion in WT-BRAF human melanoma cells on collagen I. A. Cell morphology assessment on collagen I of hMCs upon MGRN1 depletion. Representative immunoblots of MGRN1 depletion in hMCs, using GAPDH as loading control, and bright-field images of hMCs on top of atelopeptide bovine collagen I after silencing MGRN1 (72 h). Scale bar 50 μm. Bottom left: In WT-BRAF melanoma cells (HBL, MM28 and DOR), quantification of the area of cellular clusters, where dots represent the area of one cellular aggregate (n = 3, error bars are mean ± SEM, *Mann-Whitney U* test was used to generate *P* values, $*P < 0.05$ and $**P < 0.01$). Bottom right: In mutant-BRAF melanoma cells, quantification of the percentage of dendritic and rounded cells in MGRN1-deleted cells (n = 4, error bars are mean ± SEM, *Welch's t*-test was used to generate *P* values, $**P < 0.01$). **B.** Phase-contrast images of MGRN1-null cells seeded on plastic flasks (left, scale bar 50 μm) and quantification of percentage of rounded and dendritic cells (right, n = 3, error bars are mean ± SD, ANOVA test with Dunnett's multiple comparisons was used to generate *P* values, $*P < 0.05$ and $**P < 0.01$). **C.** Phase-contrast images of MGRN1-KO cells seeded on collagen I in complete medium (left, scale bar 50 μm), quantification of percentage of individual cells and cell aggregates (middle, n = 3, error bars are mean ± SD, ANOVA test with Dunnett's multiple comparisons was used to generate *P* values, $*P < 0.05$ and $**P < 0.01$) and quantification of cellular clusters area (right). Each dot represents a cellular aggregate and histogram shows the median of the area (n = 4, N = 454 cellular clusters, Kruskal Wallis test with Dunn's multiple comparisons was used to generate *P* values, $***P < 0.001$ and $****P < 0.0001$). **D.** Representative phase-contrast images (left) and quantification (right) of HBL control and MGRN1-null cells wound closure (%). White line corresponds to time point 0 h and red line to 24 h after migration. Error bars are mean ± SEM (n = 3 independent experiments) and Kruskal Wallis test with Dunn's multiple comparisons was used to generate *P* values, $*P < 0.05$. **E.** Percentage of adhesion of MGRN1 depleted cells to a collagen I matrix after 1 h. Data are referred to control cells. Error bars are mean ± SEM (n = 3 independent experiments, N = 10 replicates) and Kruskal Wallis test with Dunn's multiple comparisons was used to generate *P* values, $*P < 0.05$, $**P < 0.01$ and $****P < 0.0001$). **F.** Phase-contrast images of melanoma spheroids seeded in a collagen I matrix (scale bar 0.2 mm). White line indicates spheroids area at time point 0 and red line after 4 days of growth. Graph represents the increased area normalized to control cells and each dot corresponds to a single spheroid (n = 2 independent experiments, N = 17 spheroids, Kruskal Wallis test with Dunn's multiple comparisons was used to generate P values, $***P < 0.001$ and $****P < 0.0001$).

percentage of cells growing as cell aggregates (Fig. 1 A, bottom panels, and Supplemental Fig. 1C). In contrast, BRAF mutant cell lines (BEU and C8161) displayed a mixed morphology of elongated/mesenchymal-like and rounded/amoeboid-like cells, and MGRN1 knockdown decreased the percentage of rounded/amoeboid-like cells (Fig. 1A, bottom panels).

On one hand, these results suggested a likely differential morphology of human melanoma cells on collagen I depending on the *BRAF* status, a hypothesis which requires further investigations. On the other hand, repression of MGRN1 in WT-BRAF melanoma cells resulted in increased intercellular adhesion on collagen I, indicating that MGRN1 might modulate the expression of cell-cell adhesion molecules, which we aimed to study in more detail. It is also worth noting that this phenotype switch is the opposite event that takes place during melanoma progression, in which tumor cells change expression of adhesion molecules to promote migration and invasion, a process reminiscent of the EMT-like program [31,32].

In order to investigate the regulation of intercellular adhesion observed in WT-BRAF melanoma cells grown on collagen I upon MGRN1 ablation, we chose HBL cells as cellular model. We had previously generated MGRN1-knockdown stable clones of HBL cells by the CRISPR-Cas9 system [12]. *MGRN1* edition was achieved by transfecting a plasmid expressing nuclear Cas9 from *Streptococcus pyogenes*. This plasmid also contained a sgRNA oligo insert, bearing the 20-nt guide sequence of *MGRN1* exon 1, underlined in blue in Supplemental Fig. 1D. Consequent selection of transfected cells with puromycin allowed for the generation of MGRN1-null stable clones. We selected three independent stable clones, designated as 2.1, 3.7 and 4.9. MGRN1 knockdown was confirmed by Western blot analysis (Supplemental Fig. 1E). The details of *MGRN1* gene edition for clones 3.7 and 4.9 are shown in Supplemental Fig. 1F, resulting in truncated MGRN1 proteins in *MGRN1*-KO clones. Electropherogram of *MGRN1* gene sequencing of clone 2.1 had many overlapping peaks, which prevented accurate determination of MGRN1 edition. Lack of all relevant functional domains in MGRN1 in stable clones ensured complete loss of function of the short, truncated proteins.

Consistent with previous results in mouse melanoma cells, persistent deletion of MGRN1 in HBL melanoma cells induced a more differentiated morphology with more dendritic cells, when cells were grown on plastic flasks compared with controls (Fig. 1B). Moreover, assessment of cell morphology on collagen I revealed that loss of MGRN1 caused a decrease in the percentage of individual cells (statistically significant for clones 3.7 and 4.9) and the formation of bigger cellular aggregates in all the clones tested compared to control cells (Fig. 1C). Interestingly, visualization of time-lapse microscopy images suggested that formation of bigger cellular clusters in MGRN1-null cells occurred due to the movement of these aggregates towards nearby clusters (Supplemental videos 1–4). Furthermore, analysis of cell migration using the circular wound healing assay revealed that whereas the very modest decrease for 3.7 cells did not reach significance, MGRN1-KO clones 2.1 and 4.9 migrated significantly slower than control cells (Fig. 1D). We also investigated the ability of MGRN1-KO cells to adhere to a thick layer of collagen I and found significantly increased adhesion to this matrix for MGRN1-null cells with respect to control cells (Fig. 1E). In addition, melanoma spheroids of MGRN1-KO cells generated with the hanging drop method were embedded in a thick layer of collagen I and invasive growth capacity was measured. No significant differences in the increase of the area of the spheroids was found in clone 3.7, as in the 2D migration assay. Importantly, lack of MGRN1 (in clones 2.1 and 4.9) decreased invasive growth of melanoma spheroids compared to control cells (Fig. 1F).

To elucidate which molecular changes could be related with this *in vitro* phenotypic change mediated by MGRN1 knockdown, samples of control cells and MGRN1-KO clone 4.9 were subjected to RNA sequencing (RNA-seq) and gene set enrichment analysis (GSEA) of gene expression was performed. Volcano plot in Fig. 2A displays the results of RNA-seq of MGRN1-KO cells versus control cells, indicating upregulated genes (in red) and downregulated genes (in blue). MGRN1 expression value is highlighted in purple, serving as positive control. Of note, the number of downregulated genes is much higher than the number of upregulated genes following MGRN1 knockdown. Interestingly, GSEA of RNA-seq results revealed several upregulated gene sets in MGRN1-null cells with respect to control cells related with cell-cell and cell-matrix adhesion, modulation of GTPases and WNT-β-catenin pathway (e.g., adherens and tight junctions, integrin binding, GTP dependent protein binding, β-catenin binding; Fig. 2B and **C**). On the other hand, "Epithelial to mesenchymal transition" was among the top ranked downregulated gene sets in MGRN1-KO cells (Fig. 2B and **C**), indicating that absence of MGRN1 likely contributed to a less aggressive phenotype of melanoma cells. Moreover, we selected a custom list of genes involved in cell adhesion and their corresponding RNA-seq data were represented in a heat map and highlighted in the volcano plot, stressing that MGRN1 deletion led to a change in the profile of important cell adhesion molecules (Fig. 2A and **D**). These data strongly supported the hypothesis that MGRN1 repression regulates cellular adhesion in melanoma, at least in part by modulating the expression of intercellular adhesion molecules.

3.2. Regulation of E-cadherin expression by MGRN1

Based on the RNA-seq analysis and the functional assays shown above, we investigated whether MGRN1 could regulate expression of proteins involved in cell-cell and cell-matrix adhesion. We focused on key molecules known to be involved in these processes, whose mRNA levels were significantly upregulated in MGRN1-KO cells compared with

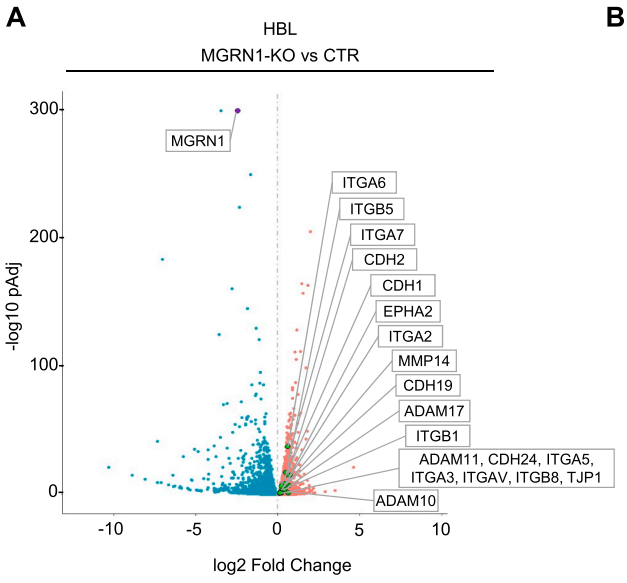

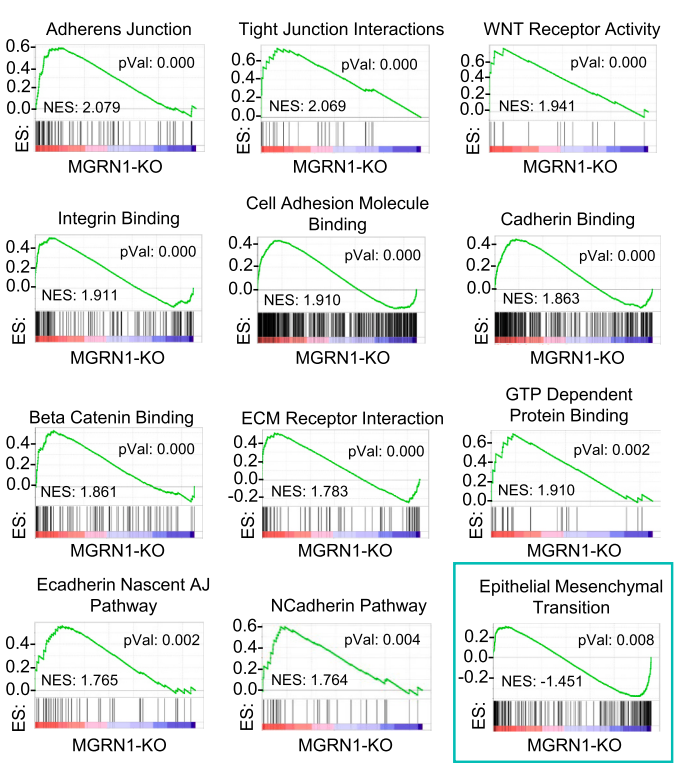

C

NAME	NES	RANK	SIZE	NOM-pVal	FDR-q
C2. KEEG. ADHERENS JUNCTION	2.08	4/173	73	0.000	0.002
C2. REACTOME. TIGHT JUNCTION INTERACTIONS	2.07	11/1012	23	0.000	0.003
C5. GO. MOLECULAR FUNCTION. WNT RECEPTOR ACTIVITY	1.94	7/791	16	0.000	0.020
C5. GO. MOLECULAR FUNCTION. INTEGRIN BINDING	1.91	14/791	138	0.000	0.016
C5. GO. MOLECULAR FUNCTION. CELL ADHESION MOLECULE BINDING	1.91	16/791	514	0.000	0.014
C5. GO. MOLECULAR FUNCTION. CADHERIN BINDING	1.86	18/791	314	0.000	0.024
C5. GO. MOLECULAR FUNCTION. BETA CATENIN BINDING	1.86	19/791	85	0.000	0.024
C2. KEEG. ECM RECEPTOR INTERACTION	1.78	20/173	79	0.000	0.001
C3.GO. MOLECULAR FUNCTION. GTP DEPENDENT PROTEIN BINDING	1.91	15/791	22	0.002	0.015
C2. PID. ECADHERIN NASCENT AJ PATHWAY	1.77	17/184	39	0.002	0.032
C2. PID. NCADHERIN PATHWAY	1.76	18/184	32	0.004	0.030
H. HALLMARK. EPITHELIAL MESENCHYMAL TRANSITION	-1.45	5/50	191	0.008	0.064

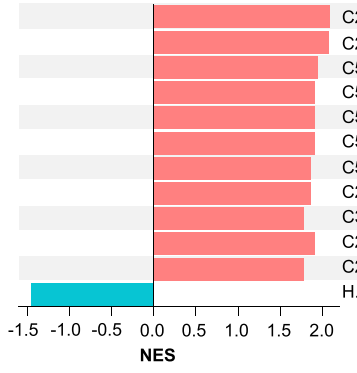

D

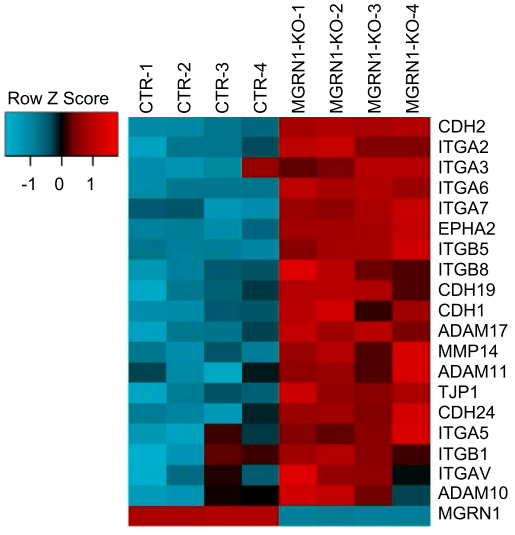

(caption on next page)

Fig. 2. Transcriptomic analysis of MGRN1-KO HBL human melanoma cells. A. Volcano plot of differentially expressed genes in MGRN1-KO cells with respect to HBL control cells (red indicates upregulated genes and blue downregulated genes). MGRN1 (in purple) and cell adhesion-related genes (in green) are highlighted. **B.** Gene set enrichment analysis (GSEA) of the RNA-seq data between MGRN1-KO and control cells (nominal p values and normalized enrichment score, NES, are shown on each gene set). **C.** List of gene sets enriched in MGRN1-deficient cells compared with control cells, related with cell adhesion, WNT signaling and GTPase modulation. Gene sets are ranked according to nominal p value (NOM-pVal) and the NES. For each gene set, molecular signature database collection, name of gene set, NES, ranked position within the molecular signature, size of the gene list, NOM-pVal and False discovery rate q value (FDR-q) are indicated. **D.** Heat map of cell adhesion gene expression after MGRN1 deletion in HBL human melanoma cells. Selected genes are ordered from top to bottom in *Y* axis according to their fold change value. Expression values are represented in color intensities according to the Row Z score: red (positive) and blue (negative).

control cells, namely E-cadherin, neural (N)-cadherin and ZO-1 (Zonula Occludens 1). These proteins are important components of cell-matrix adhesion and cell-cell interactions [33,34] and might contribute to modulate the intercellular adhesion of MGRN1-KO malignant cells. We also included connexin-43 (Gap Junction Alpha 1, GJA1), as overexpression of this gap junction protein has been reported to reduce melanoma metastatic capability [35–37]. Moreover, changes in the expression of E− and N-cadherins have already been reported in melanoma during the phenotype switch that confers metastatic properties to melanoma cells in the EMT-like process [31,32]. Progression of epidermal melanocytic lesions involves a shift from expression of E-cadherin to expression of N-cadherin, which promotes invasion into the dermis [18,19]. Consistent with this possibility, Western blot analysis showed that MGRN1-KO cells expressed higher levels of E-cadherin (Fig. 3A), the main component of adherens junctions at cell–cell and cell–matrix junctions in epithelial tissues. Regarding N-cadherin expression, there were no significant changes in any of the three MGRN1-KO clones tested (Supplemental Fig. 2A). Besides, we found no significant upregulation in GJA1 protein levels by Western blot (Supplemental Fig. 2A) or in ZO-1 protein levels by immunofluorescence (Supplemental Fig. 2B), suggesting that GJA1 and ZO-1 could not account for the increased intercellular adhesion observed upon MGRN1 deletion. Thus, we further investigated E-cadherin modulation by MGRN1.

Cell surface expression of E-cadherin was assessed by immunocytochemistry using 0.1 % saponin to avoid nuclear permeabilization and to preserve plasma membrane integrity. For the three independent MGRN1-KO clones under study, confocal images and signal intensity quantification confirmed a statistically significant increase of cell surface expression of E-cadherin in MGRN1-depleted cells compared with control cells and higher co-localization with F-actin (Fig. 3B), indicative of the association of E-cadherin-catenin complexes to the actin cytoskeleton, which is crucial for the ability of the cells to adhere to each other. The amount of E-cadherin at the plasma membrane determines the strength of adherens junctions and depends on its gene expression, protein stability and intracellular trafficking. E-cadherin reaches the cell surface through the synthetic secretory pathway and is internalized to be recycled or degraded. Thus, in addition to upregulating *CDH1* mRNA abundance, MGRN1 could modulate E-cadherin expression at different levels. To test whether E-cadherin protein stability was altered upon MGRN1 knockdown, we incubated MGRN1-KO cells with the protein synthesis inhibitor cycloheximide for different time points ranging from 6 to 24 h and protein stability was evaluated by Western blot analysis. We found that the half-life of E-cadherin did not significantly increase in MGRN1-null cells (Fig. 3C and D), thus suggesting that induction of E-cadherin following MGRN1 knockdown is not due to a stabilization of the protein. Hence, we sought to confirm a transcriptional regulation of E-cadherin by MGRN1, suggested by the RNA-seq results. qPCR measurements confirmed that the levels of *CDH1* mRNA were higher in MGRN1-KO cells compared with controls and the magnitude of this induction was comparable with the increase of E-cadherin protein abundance in the different MGRN1-KO clones (Fig. 3E). Therefore, induction of E-cadherin was not due to stabilization of the protein, and most likely depended on a transcriptional mechanism. Two classical transcriptional repressors of *CDH1* gene expression, ZEB1 and SLUG [38], were analyzed by Western blot. Interestingly, we found repression of ZEB1 protein levels in MGRN1-null cells compared with control cells, which could account for the decrease in E-cadherin expression (Fig. 3F). No significant change in SLUG protein levels was detected after MGRN1 knockdown (Fig. 3F). Thus, decreased levels of ZEB1 in the absence of MGRN1 could contribute to the increase in E-cadherin expression upon MGRN1 deletion.

The intracellular domain of E-cadherins contains binding sites to interact with catenins and other regulatory proteins. We first tested whether P120 binding to E-cadherin could participate on E-cadherin complexes at the plasma membrane and strengthen cell-cell adhesion. P120 subcellular distribution, protein expression and co-localization with E-cadherin was assessed by immunofluorescence in saponin-permeabilized cells. We found no relevant differences in protein expression in MGRN1-KO cells versus control cells (Supplemental Fig. 3A). Spatial co-localization with E-cadherin at the plasma membrane increased moderately upon MGRN1 deletion only in clone 3.7 (Supplemental Fig. 3A), suggesting a minor involvement of binding of P120 to E-cadherin at the cell surface in the enhancement of cell-cell adhesion in MGRN1-null cells.

On the other hand, binding of β-catenin to the cytoplasmic region of E-cadherin connects E-cadherin to the actin cytoskeleton and stabilizes adherens junctions [39]. To confirm the induction of E-cadherin expression at the plasma membrane in MGRN1-null cells, we evaluated the co-localization of E-cadherin and β-catenin by immunostaining using the experimental conditions described above. Confocal images and co-localization analysis showed that the percentage of co-localization between E-cadherin and β-catenin (Manders' coefficient) significantly increased in two MGRN1-KO clones compared with control cells (Fig. 4A), consistent with the increase in cell surface expression of E-cadherin upon MGRN1 deletion. Subcellular distribution of β-catenin is essential for its biological function as transcription factor. Retention of β-catenin at the plasma membrane might affect nuclear translocation of β-catenin, resulting in changes in gene expression. To test this possibility, we analyzed β-catenin subcellular distribution by immunofluorescence in MGRN1-null cells and quantified the percentage of nuclear β-catenin. We found a significant reduction in the percentage of β-catenin in the nuclei after persistent loss of MGRN1 (Fig. 4B). These results suggested that the association of β-catenin with E-cadherin at the plasma membrane in MGRN1-KO cells resulted in changes in its subcellular distribution, with decreased β-catenin translocation to the nucleus. Moreover, cell fractionation analysis using the cytoskeleton (CSK) buffer to extract nuclear chromatin-bound proteins revealed a trend towards decreased amount of chromatin-bound β-catenin in MGRN1-KO cells compared to control cells (Supplemental Fig. 3B). However, gene expression analysis of a panel of β-catenin inducible genes revealed a trend towards an increased expression of AXIN2, MITF, TCF7, cMYC and LEF1 in MGRN1-KO cells with respect to control cells (Supplemental Fig. 3C). Therefore, the decreased percentage of nuclear localization and of β-catenin chromatin-bound observed upon MGRN1 knockdown did not lead to a regulation of canonical β-catenin transcriptional activity. Accordingly, downregulation of ZEB1 in MGRN1-KO cells might be carried out primarily at a posttranscriptional level.

To further confirm that the phenotypic effects upon MGRN1 knockdown were directly related to the lack of expression of MGRN1, we performed rescue experiments overexpressing MGRN1-S(+) isoform fused to CFP in clone 2.1. HBL human melanoma cells express four MGRN1 isoforms [1]. For these experiments, we selected isoform S(+), designated S for the short version of exon 17, and (+) for expressing

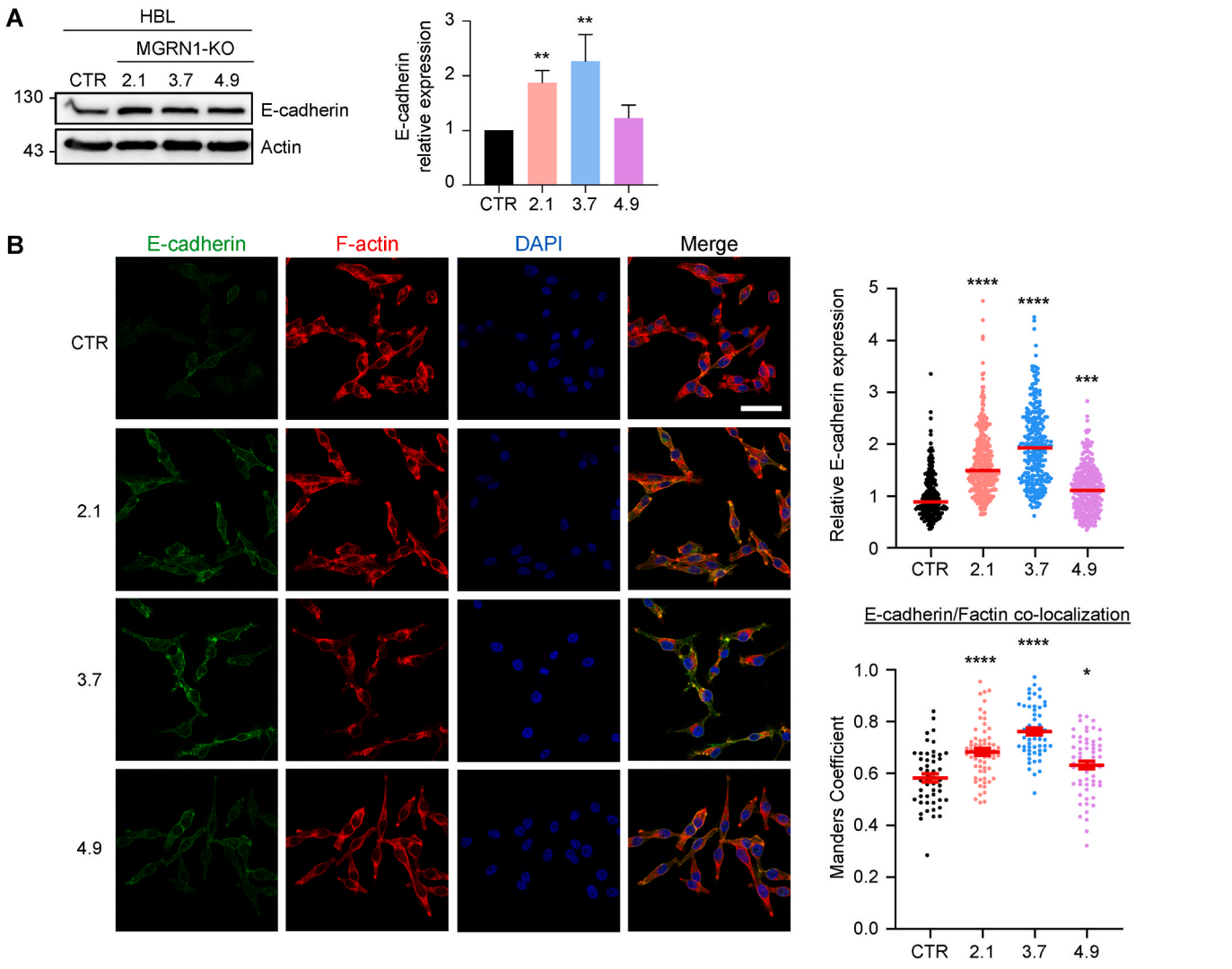

(caption on next page)

Fig. 3. Induction of E-cadherin expression upon MGRN1 knockdown in melanoma cells. A. Immunoblot and quantification of E-cadherin protein levels (n = 8, mean ± SEM, Kruskal Wallis test with Dunn's multiple comparisons was used to generate *P* values, $^{**}P < 0.01$). **B.** Confocal images of E-cadherin (green) and quantification. F-actin (red) and DAPI (blue) were also stained. Scale bar 50 μm. Each dot represents a single cell (n = 3, N = 325 cells, median, Kruskal Wallis test with Dunn's multiple comparisons was used to generate *P* values, $^{***}P < 0.001$ and $^{****}P < 0.0001$). E-cadherin/F-actin co-localization quantification using Manders' coefficient (bottom). Each dot represents a single image (n = 4, N = 50 images, mean ± SEM, ANOVA test with Dunnett's multiple comparisons was used to generate *P* values, $^{*}P < 0.05$ and $^{****}P < 0.0001$). **C.** E-cadherin immunoblots after treatment with cycloheximide (0.1 mM) for different times (CTR n = 4, 2.1 n = 3, 3.7 n = 2 and 4.9 n = 2). **D.** Semi-log of residual signals of **C** were plotted against time for calculation of half-lives (t½), corresponding to the slope of the resulting lines. **E.** Relative expression of *CDH1* estimated by qPCR (n = 5, mean ± SEM, ANOVA test with Dunnett's multiple comparisons was used to generate *P* values, $^{**}P < 0.01$). **F.** ZEB1 (left, n = 4) and SLUG (right, n = 3) immunoblots and quantification (mean ± SEM, ANOVA test with Dunnett's multiple comparisons was used to generate *P* values, $^{**}P < 0.01$). See also Supplemental Fig. 2.

exon 12, which contains a nuclear localization signal [1] (UniProt accession number O60291-1). Immunostaining analysis of E-cadherin expression and β-catenin nuclear localization revealed that overexpression of MGRN1 in MGRN1-KO clone 2.1 significantly decreased E-cadherin expression levels (Fig. 5A) and increased the percentage of nuclear β-catenin (Fig. 5B). These data strongly support that the increased E-cadherin-mediated intercellular adhesion was regulated by permanent knockdown of MGRN1.

3.3. Silencing of E-cadherin in MGRN1-KO melanoma cells reverts the regulation of cell-cell adhesion on collagen I

To investigate the contribution of E-cadherin induction to the increased dendricity of the cells seeded on plastic flasks and increased cell-cell adhesion on collagen I after MGRN1 knockdown, we depleted E-cadherin expression in MGRN1-KO cells using a mixture of three siRNAs (siE) and assessed cell morphology on 2D systems and on a collagen I matrix. Effective E-cadherin ablation was evaluated by Western blot (Fig. 6A). E-cadherin silencing in MGRN1-KO cells caused no significant effect on cell morphology when cells were seeded on plastic (Fig. 6B). However, loss of expression of E-cadherin decreased the size of cellular aggregates in MGRN1-null cells seeded on a thick layer of collagen I (Fig. 6C), suggesting the relevance of E-cadherin-mediated adherens junctions on the increased intercellular adhesion observed after depletion of MGRN1. Furthermore, we used individual siRNAs targeting E-cadherin transcripts (A, B and C) and confirmed that repression of E-cadherin in MGRN1-KO cells decreased the area of cellular clusters, thus reverting the enhanced intercellular adhesion after MGRN1 knockdown (Supplemental Fig. 4A). We also examined β-catenin protein levels and subcellular localization in MGRN1-KO cells upon E-cadherin knockdown and found no significant effect on β-catenin protein levels in E-cadherin-depleted MGRN1-null cells compared with control cells (Supplemental Fig. 4B). Interestingly, the decrease in the percentage of nuclear β-catenin upon MGRN1 depletion appeared to be modulated by E-cadherin (Supplemental Fig. 4C), confirming our previous observations.

3.4. E-cadherin upregulation decreased CDC42 activation in MGRN1-KO cells

Given the role of Rho-GTPases in cytoskeletal dynamics and the functional interaction of cadherin receptors with small GTPases in adherens junctions, we studied the potential relevance of two Rho-GTPases, RAC1 and CDC42, in MGRN1-KO cells phenotype. Pharmacological inhibition of either RAC1 or CDC42 GTPases resulted in larger cellular aggregates in control cells seeded on collagen I matrix, but only CDC42 inhibition had a comparable and significant effect on MGRN1-null cells (Fig. 7A). We performed these assays in MGRN1-KO clone 2.1 as cellular model of MGRN1 depletion. Therefore, inhibition of RAC1 and CDC42 phenocopied the effect of MGRN1 depletion in melanoma cells and inhibition of CDC42 after MGRN1 knockdown further increased intercellular adhesion. As Rho-GTPases are also critical regulators of E-cadherin in adherens junctions, we sought to determine whether RAC1 and CDC42 could at the same time regulate expression of E-cadherin. We found that inhibition of RAC1 and CDC42 had no significant effect on E-cadherin protein levels in control cells and no further increase in E-cadherin was observed in MGRN1-KO cells (clone 2.1) after inhibition of RAC1 or CDC42 (Fig. 7B). Thus, RAC1 or CDC42 inhibition of control and MGRN1-KO cells did not lead to modulation of E-cadherin levels.

To assess whether loss of MGRN1 could modulate Rho-GTPases activation, we performed pulldown assays of RAC1 and CDC42 in MGRN1-deficient cells. We found no significant difference in RAC1 activation, but reduced levels of active GTP-bound CDC42 in all three clones (Fig. 7C), suggesting that absence of MGRN1 might decrease CDC42 activity and contribute to the increased intercellular adhesion observed in MGRN1-null cells. Since Rho-GTPases can be regulated by downstream signaling from cell-cell adhesion receptors, we investigated whether E-cadherin upregulation in MGRN1-depleted cells also modulated CDC42 activation. We silenced E-cadherin expression with a mixture of siRNAs in control and MGRN1-KO cells and evaluated CDC42 activation by a pulldown assay. E-cadherin knockdown abolished the decrease in CDC42 activation in MGRN1-deleted cells (Fig. 7D), indicating that upregulation of E-cadherin could be involved in the inhibition of CDC42 mediated by MGRN1 repression. To further confirm the signaling pathway "loss of MGRN1→upregulation of E-cadherin→inhibition of CDC42→enhanced intercellular adhesion in melanoma cells", we silenced E-cadherin with siRNAs and inhibited CDC42 activity to check cellular morphology on collagen I. We found that in control and in MGRN1-KO cells, depletion of E-cadherin abolished the aggregation-promoting effect of CDC42 inhibition (Fig. 7E). These data further support the notion that E-cadherin induction and CDC42 inhibition are molecular events lying in the pathway linking MGRN1 deficiency with increased cell-cell adhesion. The activity of CDC42 is partly regulated by GAPs. We explored the possibility that repression of MGRN1 may induce the expression of a CDC42-GAP. To test this hypothesis, we analyzed ARH-GAP17 and RAC-GAP1 protein levels, but we found no significant change in the expression of these GAPs (Supplemental Fig. 4D), suggesting that regulation of CDC42 activity after MGRN1 deletion may engage other GAPs or another molecular mechanism. Overall, our results show that MGRN1 expression is an important determinant of melanoma cell morphology and intercellular aggregation. These effects are heavily dependent on the NRAS and BRAF mutational status (Fig. 8A) and involve a MGRN1-dependent regulation of E-cadherin expression, with modulation of CDC42 activity in an ARH-GAP17/RAC-GAP1 independent manner (Fig. 8B). Therefore, MGRN1 seems to be an important player in the EMT-like transition leading to melanoma metastasis.

4. Discussion

Metastasis is the leading cause of death in cancer patients. The EMT is crucial in metastasis of epithelial cancers. In melanoma, a similar process of phenotype switching has been described, designated as EMT-like program [40]. One of the features of this EMT-like in melanomas is a switch in the expression of cell adhesion molecules.

In this study, we demonstrate for the first time that WT-BRAF melanoma cells show a clustering-like morphology on a collagen I matrix, resembling the structural behavior of epithelial cells [41]. This was an observation not previously reported since most cell morphology assays of melanoma cells were performed using mutant-BRAF cell lines. In line

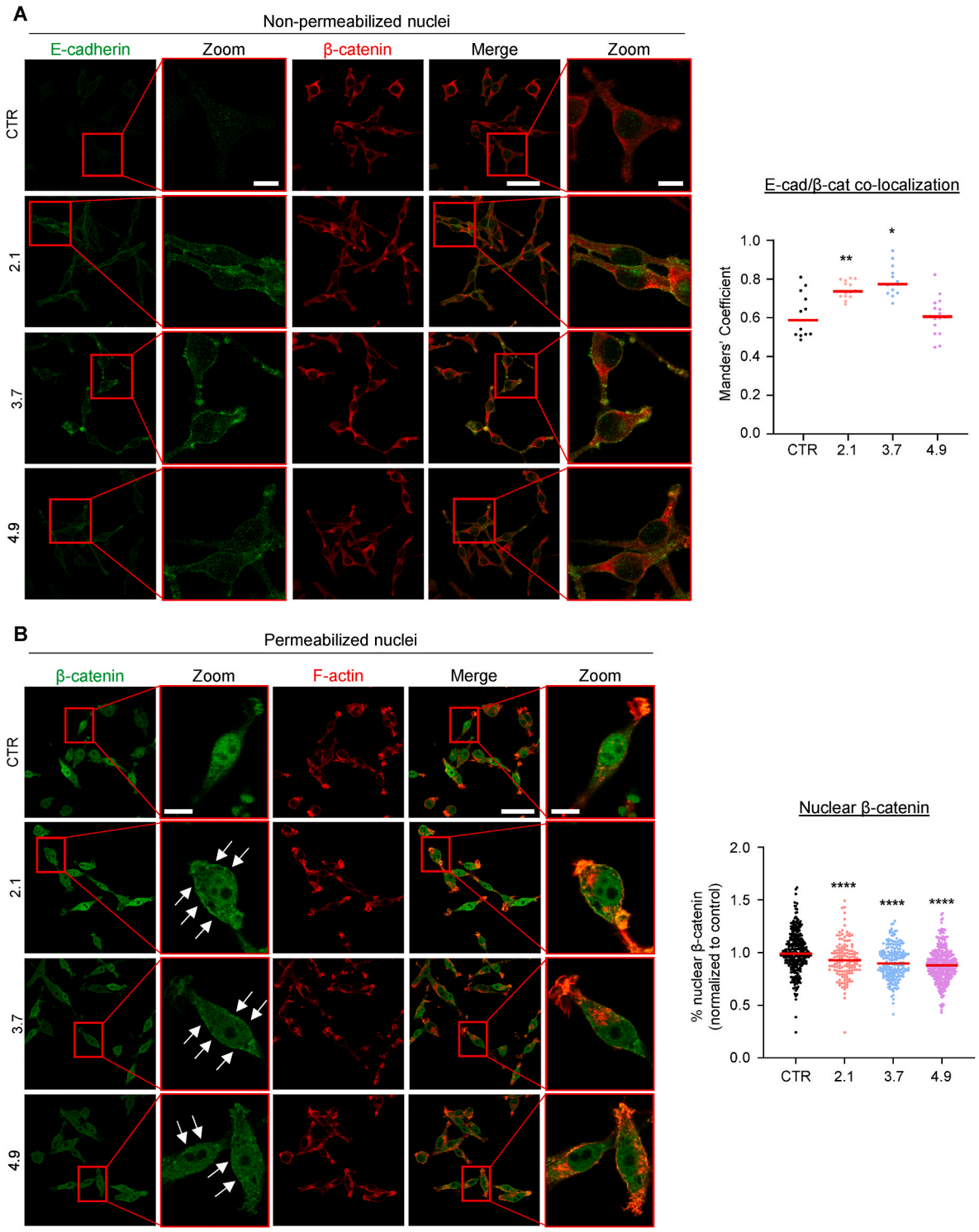

Fig. 4. Increased co-localization of E-cadherin and β-catenin in MGRN1-deficient cells. A. Representative confocal image (left) of E-cadherin (green) and β-catenin (red) immunofluorescence stainings using non-permeabilized nuclei conditions (0.1 % saponin) and quantification of co-localization using the Manders' coefficient (right) of HBL MGRN1-null cells. Scale bar 50 μm and 20 μm in zoomed images. Each dot represents a single image. The graph shows the median of the Manders' coefficient (n = 2 independent experiments, N = 12 images, Kruskal Wallis test with Welch's correction and Dunn's multiple comparisons was used to generate *P* values, $^{*}P < 0.05$ and $^{**}P < 0.01$). **B.** Representative confocal images (left) and quantification (right) of β-catenin (green) subcellular localization using 0.1 % Triton to permeabilize plasma and nuclear membrane. F-actin was stained in red. Scale bar 50 μm and 10 μm in zoomed images. White arrows stress membrane-associated staining. Each dot in the histogram represents a single cell and the graph shows the median of the percentage of nuclear β-catenin (n = 3 independent experiments, N = 142 cells, Kruskal Wallis test with and Dunn's multiple comparisons was used to generate *P* values, $^{****}P < 0.0001$). See also Supplemental Fig. 3.

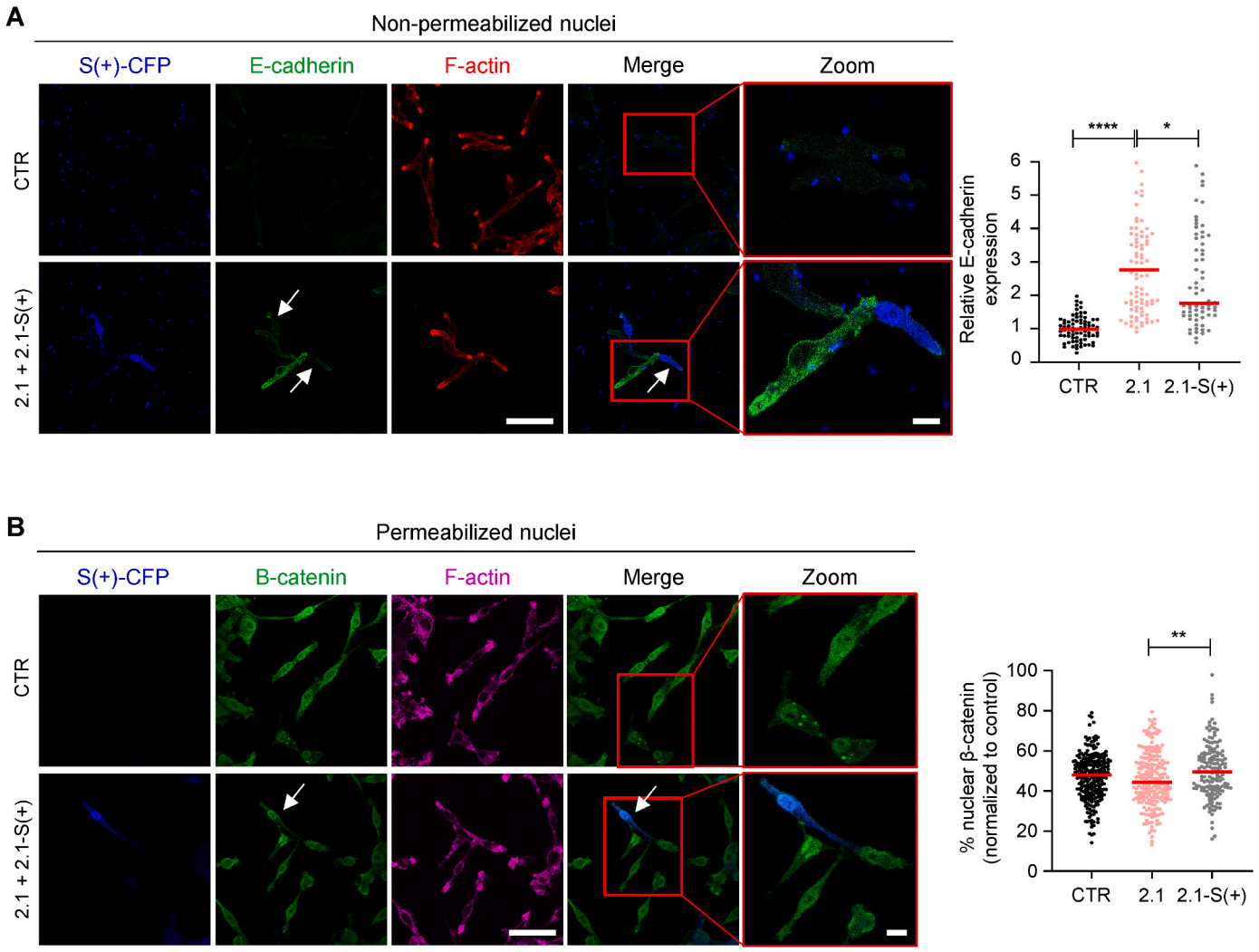

Fig. 5. MGRN1 overexpression restored E-cadherin levels and β-catenin nuclear localization in MGRN1-null cells. A. Representative confocal images (left) of E-cadherin (green) after MGRN1-S(+)-CFP (blue) overexpression in MGRN1-KO clone 2.1 using non-permeabilized nuclei conditions (0.1 % saponin). F-actin is also stained in red. Merge images correspond to S(+)-CFP + E-cadherin. Scale bar 50 μm and 10 μm in zoomed images. Graph shows the median of E-cadherin levels, and each dot represents a single cell (n = 2 independent experiments, at least 66 cells/condition, Mann-Whitney U test was used to generate P values, *$P < 0.05$ and ****$P < 0.0001$). **B.** Representative confocal images (left) and quantification (right) of β-catenin (green) subcellular localization in control cells and after MGRN1-S(+)-CFP (blue) overexpression, using 0.1 % Triton to permeabilize membrane and nuclei. F-actin was stained in pink. Merge images correspond to S(+)-CFP + β-catenin. Scale bar 50 μm and 10 μm in zoomed images. Graph shows the median of the percentage of nuclear β-catenin and each dot represents a single cell (n = 5 independent experiments, N = 155 cells, Mann-Whitney U test was used to generate P value, **$P < 0.01$).

with these results, some studies have reported that mutant BRAF signaling resulted in a decrease in E-cadherin levels and enhanced invasion in melanoma [42] and in thyroid cancer cells [43]. In contrast, the NRAS mutant melanoma cell line DOR shows an intermediate phenotype between WT-BRAF and mutant-BRAF melanoma cells, with small cellular aggregates. These observations will require further investigations to elucidate the underlying molecular mechanism.

Interestingly, gene set enrichment analyses of MGRN1-null cells versus control cells revealed a panel of enriched gene sets involved in cell-cell and cell-matrix adhesion, WNT signaling pathway and modulation of GTPases. In addition, genes related with the EMT program were also modulated in MGRN1-KO cells versus control cells. These findings were consistent with previous evidence on mouse melanoma cell lines [13] and pointed that long term MGRN1 knockdown induces a less metastatic phenotype with changes in cytoskeleton and cell adhesion molecules. Accordingly, mRNA levels of genes coding for several cadherins and integrins were upregulated in MGRN1-KO cells, indicating a change in the expression profile of cell adhesion molecules in the absence of MGRN1. *In vitro* experiments showed that loss of *MGRN1* expression in WT-BRAF human melanoma cells promoted a differentiated phenotype, with increased cell-cell adhesion on collagen I, lower motility in 2D and decreased invasive growth in collagen I. Time-lapse movies of MGRN1-KO cells and control cells grown on collagen I indicated that bigger cellular clusters observed in the absence of MGRN1 tended to form by migration of these collective groups towards other nearby clusters. This evidence suggested that secretion of extracellular proteins might contribute to attract other cellular aggregates and form bigger groups in MGRN1-null cells. Interestingly, we have non-published data demonstrating that incubation of conditioned media secreted by normal mouse melanocytes with null expression of Mgrn1 (melan-md1 cells) induced the formation of dendrites in melan-a6 normal mouse melanocytes. The hypothesis that secretion may participate in this phenotypic switch of increased cell-cell adhesion upon MGRN1 depletion remains to be further explored.

Of note, E-cadherin total protein levels and association with the plasma membrane were upregulated upon MGRN1 depletion. Since E-cadherin expression is reduced in the early stages of melanoma progression [44], reactivation of E-cadherin levels by MGRN1 depletion

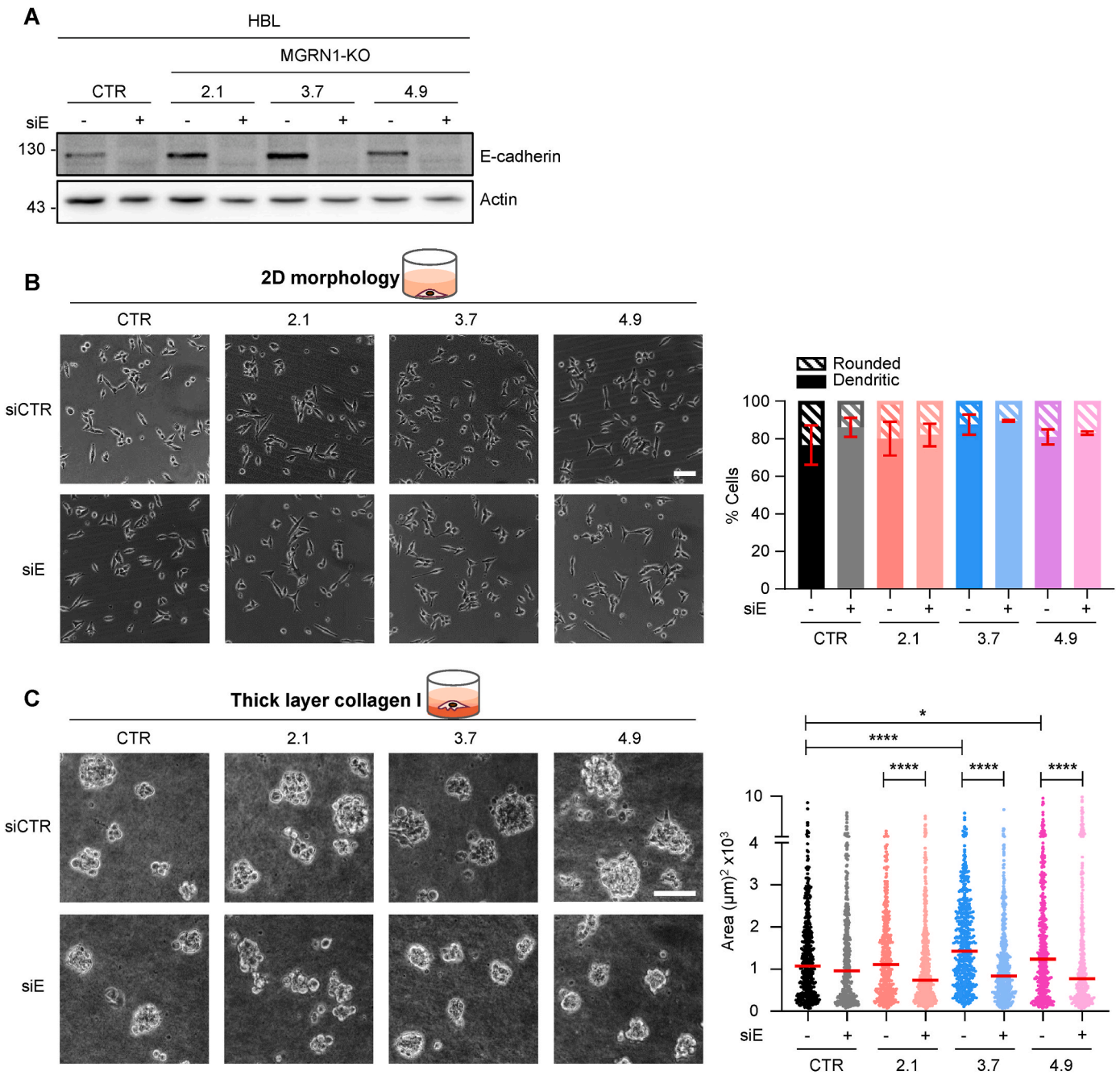

Fig. 6. Loss of E-cadherin expression abolished increased intercellular adhesion in MGRN1-null cells compared with control cells. A. Representative immunoblot of E-cadherin after knockdown of E-cadherin for 72 h in MGRN1-KO cells. β-actin (Actin) was used as loading control. **B.** Phase-contrast images (left) and quantification (right) of E-cadherin-depleted MGRN1-KO cells on plastic flasks. Scale bar 50 μm. Graph shows quantification of the percentage of rounded and dendritic cells (n = 3, error bars are mean ± SEM). **C.** Phase-contrast images (left) and quantification (right) of MGRN1-KO cells seeded on a thick layer of collagen I upon E-cadherin knockdown. Scale bar 50 μm. Each dot represents a cellular cluster and histogram shows the median area of the cellular aggregates (n = 3 independent experiments, N = 464 cellular aggregates, *Mann-Whitney t*-test was used to generate *P* values, $^{*}P < 0.05$ and $^{****}P < 0.0001$). See also Supplemental Fig. 4.

could revert the transition to a more invasive phenotype. Furthermore, we demonstrate that E-cadherin stability did not increase in the absence of MGRN1, but in contrast, mRNA levels were upregulated, suggesting a transcriptional regulation of this cadherin. Indeed, this transcriptional regulation in MGRN1-depleted cells might be due to downregulation of the EMT transcription factor ZEB1, a well-known repressor of E-cadherin expression. Moreover, increased E-cadherin expression at the plasma membrane upon MGRN1 deletion was associated with higher co-localization with F-actin and the E-cadherin intracellular interactor β-catenin. Binding of E-cadherin and β-catenin connects E-cadherin with the actin cytoskeleton and contributes to stabilize adherens junctions. Importantly, retention of β-catenin at the cell surface in MGRN1-null cells moderately decreased its nuclear translocation. It has been reported that β-catenin/TCF4 complexes bind directly to the ZEB1 promoter, inducing its expression and increasing invasiveness of cancer colon cells [45]. We hypothesize that decreased percentage of nuclear β-catenin upon MGRN1 knockdown may likely cause a reduction in ZEB1 expression and participate in the regulation of E-cadherin levels.

Transcriptomic analysis and *in vitro* experiments demonstrate the effect of absence of MGRN1 expression on cell-cell adhesion. Abrogation of E-cadherin expression in MGRN1-KO cells using 3 siRNAs, alone or in combination, reverted the increase in the area of cellular aggregates in

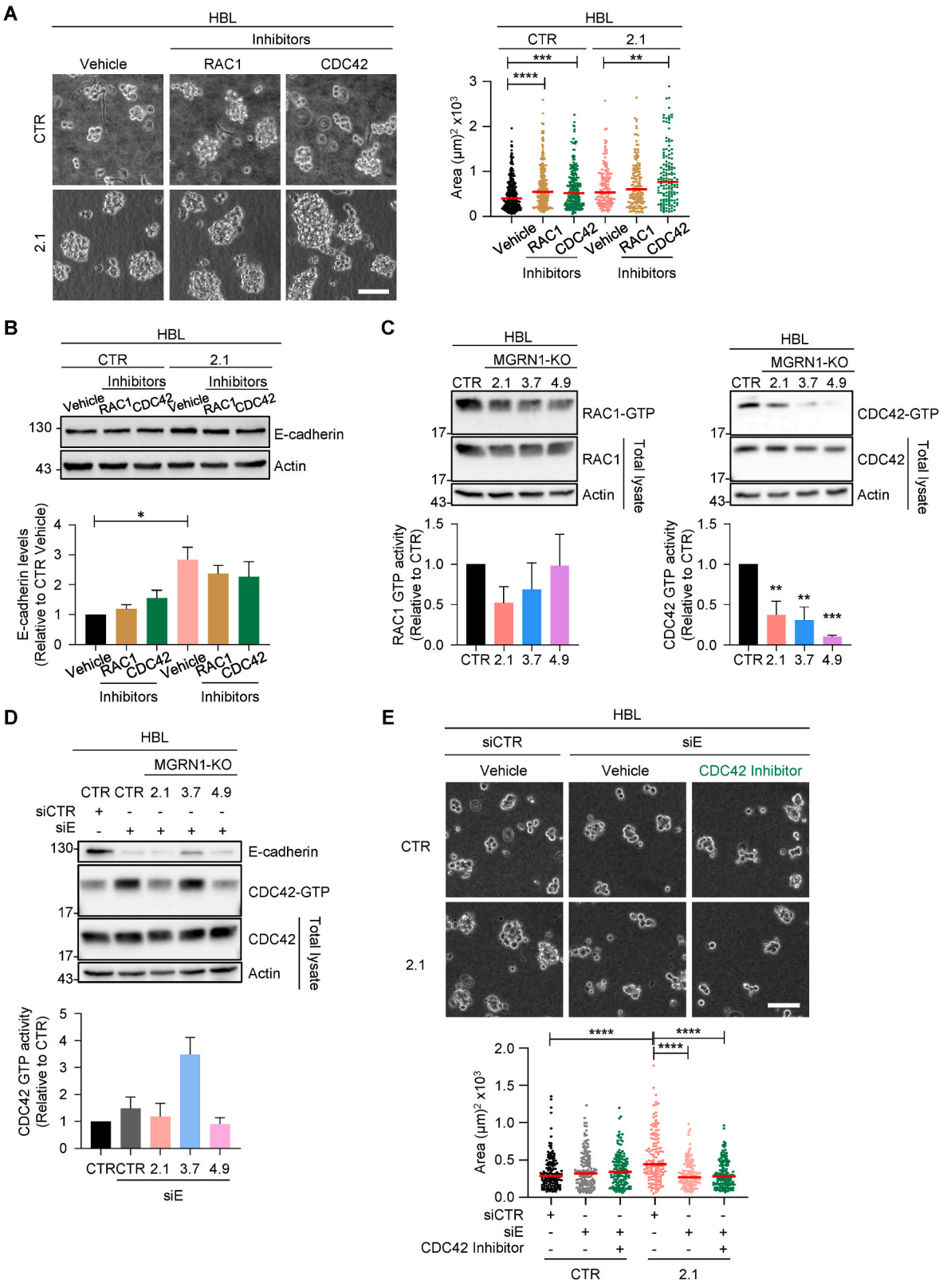

(caption on next page)

Fig. 7. E-cadherin-mediated inhibition of CDC42-GTPase activity in MGRN1-null cells. A. Phase-contrast images (left) of HBL control (CTR) and MGRN1-KO clone 2.1 seeded on a thick of collagen I in 1 % serum medium (scale bar 50 μm) after 24 h of treatment with pharmacological inhibitors of small Rho-GTPases. Quantification (right) of the area of cellular aggregates. Each dot represents a cellular aggregate and graph shows the median of the area (n = 3 independent experiments, N = 140 cellular aggregates, *Mann-Whitney U* test was used to generate *P* values, $^{**}P < 0.01$, $^{***}P < 0.001$ and $^{****}P < 0.0001$). **B.** Immunoblot (left) and quantification of E-cadherin levels upon Rho-small GTPases pharmacological inhibition. β-Actin (Actin) was used as loading control. Protein levels were measured and referred to control cells (error bars are mean ± SEM, n = 5). **C.** Representative immunoblots (top) and quantifications (bottom) of RAC1-GTPase (left) and CDC42-GTPase activity (right) in HBL MGRN1 depleted cells. Protein levels were referred to RAC1 and CDC42 total lysate of each sample and normalized to control cells (n = 4, error bars are mean ± SEM, Kruskal Wallis test with and Dunn's multiple comparisons was used to generate *P* values, $^{**}P < 0.01$ and $^{***}P < 0.001$). **D.** Immunoblot (top) and quantification (bottom) of CDC42-GTPase activity after E-cadherin silencing for 72 h using siRNAs. E-cadherin was detected to confirm effective knockdown. CDC42-GTPase activity was referred to CDC42 total lysate of each sample and normalized to control cells (error bars are mean ± SEM, n = 3). **E.** Phase-contrast images of HBL control (CTR) and MGRN1-KO clone 2.1 seeded on collagen I matrix in 1 % serum medium (scale bar 50 μm) after 24 h of treatment with RAC1/CDC42 pharmacological inhibitors and 72 h of E-cadherin silencing. Graph shows the quantification of the area of cellular aggregates where each dot represents a cellular aggregate (n = 2 independent experiments, N = 137 cellular aggregates, median). *Mann-Whitney U* test was used to generate P values, $^{****}P < 0.0001$). See also Supplemental Fig. 4.

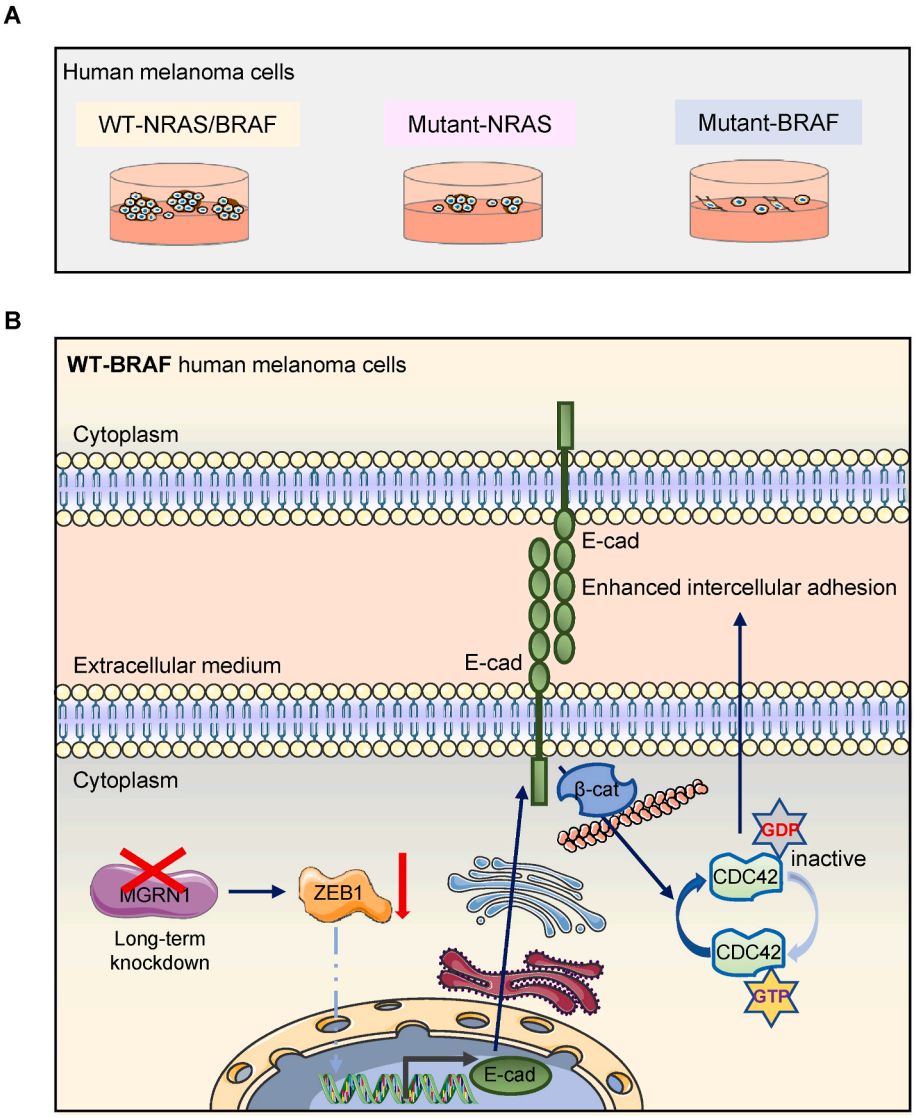

Fig. 8. Enhanced intercellular adhesion mediated by reactivation of E-cadherin and inhibition of CDC42 activity after MGRN1 depletion in melanoma cells. A. In human melanoma cells, WT-BRAF cells form cellular clusters on a collagen I matrix. NRAS-mutant cells also display cellular aggregates on collagen I, but they are smaller. On the other hand, mutant-BRAF cells show a mixed population of cells on collagen I with elongated-mesenchymal cells and rounded-amoeboid cells. **B.** In WT-BRAF human melanoma cells, permanent deletion of MGRN1 increases intercellular adhesion due partly to increased expression of E-cadherin (E-cad) at the plasma membrane, stabilizing adherens junctions, and bigger co-localization with β-catenin (β-cat). Regulation of E-cadherin occurs likely by a transcriptional mechanism because of downregulation of the EMT-transcription factor ZEB1. Finally, increased expression of E-cadherin signals intracellularly inhibiting CDC42 activity, which might contribute to the enhanced cell-cell adhesion phenotype of MGRN1-null cells.

MGRN1-KO cells grown on top of a thick layer of collagen I. These data demonstrate the contribution of E-cadherin to the enhanced intercellular adhesion observed after MGRN1 deletion. We ruled out the participation of GJA1 and ZO-1. However, we cannot exclude the role of other adhesion molecules in this phenotype. Furthermore, rescue experiments restoring MGRN1 expression by transient transfection of isoform MGRN1-S(+) in MGRN1-null cells further supported that the increase in E-cadherin expression levels and the decrease in the percentage of nuclear β-catenin in MGRN1-KO clones are directly related to MGRN1 knockdown.

On the other hand, small Rho-GTPases are key players in the regulation of actin dynamics and cell adhesion and migration [46]. Pharmacological inhibition of two important Rho-GTPases, RAC1 and CDC42, in human melanoma cells caused a similar increase of cell-cell adhesion than MGRN1 depletion, but only CDC42 inhibition increased further the area of the cellular clusters in MGRN1-KO cells on collagen I. No change in E-cadherin expression was observed in RAC1- and CDC42-inhibited control and MGRN1-KO cells, suggesting that no modulation of E-cadherin occurred downstream of RAC1 or CDC42. Furthermore, we showed that MGRN1 depletion in human melanoma cells inhibited CDC42 and this decrease in CDC42 activity appeared mediated by the increase in E-cadherin levels upon MGRN1 depletion. Moreover, the increase in the area of cellular aggregates upon CDC42 inhibition in MGRN1-KO cells was abolished after E-cadherin knockdown. Thus, loss of expression of MGRN1 in human melanoma cells leads to E-cadherin upregulation and decreased CDC42 activity, promoting intercellular adhesion.

In this study, WT-BRAF human melanoma cells were interrogated to assess the effect of permanent MGRN1 repression in melanoma progression using a combination of solid *in vitro* functional assays and RNA-seq analysis to draw the conclusion that MGRN1 is an important determinant of melanoma aggressiveness. However, *in vivo* experiments should be conducted to better demonstrate the tumorigenic role of MGRN1 in human melanoma. It is worth noting that all MGRN1 isoforms were repressed in MGRN1-KO cells, which prevented from distinguishing whether the effects observed upon MGRN1 knockdown could be isoform-specific. This might be mechanistically important in that even though all MGRN1 isoforms express exon 10 responsible for the E3 ligase activity, only MGRN1 isoforms expressing exon 12, (+) isoforms, contain a nuclear localization signal. Cytosolic localization or nuclear translocation of MGRN1 may result in different effects on melanoma cells. To address these two possibilities, mutants of the RING Finger domain of MGRN1 could be generated to evaluate the contribution of ubiquitination to this phenotypic switch induced by MGRN1 repression in melanoma cells.

Our group previously demonstrated that MGRN1 expression is higher in skin cutaneous melanoma compared with nevi and normal skin. Moreover, analysis of publicly available melanoma datasets and a preliminary study of a limited number of human melanoma biopsies strongly suggested that low MGRN1 expression in melanoma patients is associated with a longer patient survival [12]. Therefore, it is tempting to speculate that an increase in the expression of MGRN1 in nevi might contribute to the transition to a malignant phenotype by downregulating E-cadherin levels, which may foster the full transformation of nevi or normal skin to melanoma. In any case, our data strongly support the hypothesis that MGRN1 is an important regulator of human melanoma progression and that targeting MGRN1 may reactivate E-cadherin expression and contribute to reduce the EMT-like program in melanoma. Thus, MGRN1 may be considered in the clinical management of melanoma patients as a potential biomarker.

CRediT authorship contribution statement

S. Cerdido: Writing – original draft, Validation, Methodology, Investigation, Formal analysis. **M. Abrisqueta:** Investigation, Formal analysis. **J. Sánchez-Beltrán:** Formal analysis. **A. Lambertos:** Investigation. **M. Castejón-Griñán:** Investigation. **C. Muñoz:** Investigation. **C. Olivares:** Investigation. **J.C. García-Borrón:** Writing – original draft, Supervision, Project administration, Funding acquisition. **C. Jiménez-Cervantes:** Supervision, Project administration, Funding acquisition, Conceptualization. **C. Herraiz:** Writing – original draft, Supervision, Methodology, Investigation, Formal analysis, Conceptualization.

Declaration of competing interest

The authors declare that they have no known competing financial interests or personal relationships that could have appeared to influence the work reported in this paper.

Acknowledgments

This work was supported by Fondo de Investigaciones Sanitarias, Instituto de Salud Carlos III, Spain [Grant PI22/00404] and co-funded by the European Union (to C.J.-C. and J.C.G.-B.). Sonia Cerdido holds a FPI predoctoral fellowship from the University of Murcia. We thank Javier Aroca Esteban for his valuable contribution to this work and Dr. Fernando Pérez Sanz for his help with the processing of RNA-seq data.

Appendix A. Supplementary data

Supplementary data to this article can be found online at https://doi.org/10.1016/j.canlet.2023.216484.

References

[1] A.B. Perez Oliva, L.P. Fernendez, C. Detorre, et al., Identification and functional analysis of novel variants of the human melanocortin 1 receptor found in melanoma patients, Hum. Mutat. 30 (5) (2009) 811–822, https://doi.org/10.1002/humu.20971.
[2] P. Bagher, J. Jiao, C. Owen Smith, C.D. Cota, T.M. Gunn, Characterization of mahogunin ring finger-1 expression in mice, Pigm. Cell Res. 19 (6) (2006) 635–643, https://doi.org/10.1111/j.1600-0749.2006.00340.x.
[3] L.K. Phan, F. Lin, C.A. LeDuc, W.K. Chung, R.L. Leibel, The mouse mahoganoid coat color mutation disrupts a novel C3HC4 RING domain protein, J. Clin. Invest. 110 (10) (2002) 1449–1459, https://doi.org/10.1172/JCI16131.
[4] J. Sirés-Campos, A. Lambertos, Cédric Delevoye, et al., Mahogunin Ring Finger 1 regulates pigmentation by controlling the pH of melanosomes in melanocytes and melanoma cells 79 (2022) 47, https://doi.org/10.1007/s00018-021-04053-9.
[5] L. He, X.Y. Lu, A.F. Jolly, et al., Spongiform degeneration in mahoganoid mutant mice, Science 299 (2003) 710–712, https://doi.org/10.1126/science.1079694.
[6] C.D. Cota, P. Bagher, P. Pelc, C.O. Smith, C.R. Bodner, T.M. Gunn, Mice with mutations in Mahogunin ring finger-1 (Mgrn1) exhibit abnormal patterning of the left-right axis, Dev. Dynam. 235 (2006) 3438–3447, https://doi.org/10.1002/dvdy.20992.
[7] M. Abrisqueta, C. Olivares, C. Herraiz, et al., Human melanocortin 1 receptor-mediated ubiquitination of nonvisual arrestins. Role of Mahogunin Ring Finger 1 E3 ligase, Biochim. Biophys. Acta Mol. Cell Res. 1865 (1) (2018) 76–94, https://doi.org/10.1016/j.bbamcr.2017.09.013.
[8] P. Majumder, O. Chakrabarti, Mahogunin regulates fusion between amphisomes/MVBs and lysosomes via ubiquitination of TSG101, Cell Death Dis. 6 (11) (2015), https://doi.org/10.1038/CDDIS.2015.257.
[9] R. Mukherjee, A. Bhattacharya, A. Sau, S. Basu, S. Chakrabarti, O. Chakrabarti, Calmodulin regulates MGRN1-GP78 interaction mediated ubiquitin proteasomal degradation system, Faseb. J. 33 (2) (2019) 1927–1945, https://doi.org/10.1096/FJ.201701413RRR.
[10] R. Mukherjee, O. Chakrabarti, Regulation of Mitofusin1 by mahogunin ring finger-1 and the proteasome modulates mitochondrial fusion, Biochim. Biophys. Acta 1863 (12) (2016) 3065–3083, https://doi.org/10.1016/J.BBAMCR.2016.09.022.
[11] R. Mukherjee, P. Majumder, O. Chakrabarti, MGRN1-mediated ubiquitination of α-tubulin regulates microtubule dynamics and intracellular transport, Traffic 18 (12) (2017) 791–807, https://doi.org/10.1111/tra.12527.
[12] M. Abrisqueta, S. Cerdido, J. Sánchez-Beltrán, et al., MGRN1 as a phenotypic determinant of human melanoma cells and a potential biomarker, Life 12 (8) (2022), https://doi.org/10.3390/LIFE12081118.
[13] I. Martínez-vicente, M. Abrisqueta, C. Herraiz, et al., Mahogunin ring finger 1 is required for genomic stability and modulates the malignant phenotype of melanoma cells, Cancers 12 (10) (2020) 1–23, https://doi.org/10.3390/CANCERS12102840.
[14] I. Yeh, B.C. Bastian, Melanoma pathology: new approaches and classification, Br. J. Dermatol. 185 (2) (2021) 282–293, https://doi.org/10.1111/BJD.20427.

[15] S. Kuphal, A. Bosserhoff, Recent progress in understanding the pathology of malignant melanoma, J. Pathol. 219 (4) (2009) 400–409, https://doi.org/10.1002/PATH.2617.
[16] Y. Tang, S. Durand, S. Dalle, J. Caramel, EMT-inducing transcription factors, drivers of melanoma phenotype switching, and resistance to treatment, Cancers 12 (8) (2020) 1–17, https://doi.org/10.3390/CANCERS12082154.
[17] F.Z. Li, A.S. Dhillon, R.L. Anderson, G. McArthur, P.T. Ferrao, Phenotype switching in melanoma: implications for progression and therapy, Front. Oncol. 5 (FEB) (2015), https://doi.org/10.3389/FONC.2015.00031.
[18] J. Caramel, E. Papadogeorgakis, L. Hill, et al., A switch in the expression of embryonic EMT-inducers drives the development of malignant melanoma, Cancer Cell 24 (4) (2013) 466–480, https://doi.org/10.1016/J.CCR.2013.08.018.
[19] A.J. Miller, M.C. Mihm, Melanoma. N Engl J Med 355 (1) (2006) 51–65, https://doi.org/10.1056/NEJMra052166.
[20] I. Kaszak, O. Witkowska-Piłaszewicz, Z. Niewiadomska, B. Dworecka-Kaszak, F. N. Toka, P. Jurka, Role of cadherins in cancer-A review, Int. J. Mol. Sci. 21 (20) (2020) 1–17, https://doi.org/10.3390/IJMS21207624.
[21] K. Wolf, S. Alexander, V. Schacht, et al., Collagen-based cell migration models in vitro and in vivo, Semin. Cell Dev. Biol. 20 (8) (2009) 931–941, https://doi.org/10.1016/J.SEMCDB.2009.08.005.
[22] J.C. Oliveros, M. Franch, D. Tabas-Madrid, et al., Breaking-Cas-interactive design of guide RNAs for CRISPR-Cas experiments for ENSEMBL genomes, Nucleic Acids Res. 44 (W1) (2016) W267–W271, https://doi.org/10.1093/NAR/GKW407.
[23] M.I. Love, S. Anders, V. Kim, W. Huber, RNA-Seq workflow: gene-level exploratory analysis and differential expression, F1000Res 4 (2015) 1070, https://doi.org/10.12688/F1000RESEARCH.7035.1/.
[24] A. Subramanian, P. Tamayo, V.K. Mootha, et al., Gene set enrichment analysis: a knowledge-based approach for interpreting genome-wide expression profiles, Proc. Natl. Acad. Sci. U. S. A. 102 (43) (2005) 15545–15550, https://doi.org/10.1073/PNAS.0506580102.
[25] A. Liberzon, C. Birger, H. Thorvaldsdóttir, M. Ghandi, J.P. Mesirov, P. Tamayo, The Molecular Signatures Database (MSigDB) hallmark gene set collection, Cell Syst 1 (6) (2015) 417–425, https://doi.org/10.1016/J.CELS.2015.12.004.
[26] E. Hodis, I.R. Watson, G.V. Kryukov, et al., A landscape of driver mutations in melanoma, Cell 150 (2) (2012) 251–263, https://doi.org/10.1016/j.cell.2012.06.024.
[27] M. Krauthammer, Y. Kong, B.H. Ha, et al., Exome sequencing identifies recurrent somatic RAC1 mutations in melanoma, Nat. Genet. 44 (9) (2012) 1006–1014, https://doi.org/10.1038/ng.2359.
[28] E. Muñoz-Couselo, E.Z. Adelantado, C. Ortiz, J.S. García, J. Perez-Garcia, NRAS-mutant melanoma: current challenges and future prospect, OncoTargets Ther. 10 (2017) 3941–3947, https://doi.org/10.2147/OTT.S117121.
[29] A. Alqathama, BRAF in malignant melanoma progression and metastasis: potentials and challenges, Am. J. Cancer Res. 10 (4) (2020) 1103.
[30] J.C. Garcia-Borron, Z. Abdel-Malek, C. Jimenez-Cervantes, MC1R, the cAMP pathway, and the response to solar UV: extending the horizon beyond pigmentation, Pigment. Cell Melanoma Res. 27 (5) (2014) 699–720, https://doi.org/10.1111/pcmr.12257.
[31] L. Hao, J.R. Ha, P. Kuzel, E. Garcia, S. Persad, Cadherin switch from E- to N-cadherin in melanoma progression is regulated by the PI3K/PTEN pathway through Twist and Snail, Br. J. Dermatol. 166 (6) (2012) 1184–1197, https://doi.org/10.1111/J.1365-2133.2012.10824.X.
[32] D. Pedri, P. Karras, E. Landeloos, J.C. Marine, F. Rambow, Epithelial-to-mesenchymal-like transition events in melanoma, FEBS J. 289 (5) (2022) 1352–1368, https://doi.org/10.1111/FEBS.16021.
[33] M. Yulis, D.H.M. Kusters, A. Nusrat, Cadherins: cellular adhesive molecules serving as signalling mediators, J. Physiol. 596 (17) (2018) 3883–3898, https://doi.org/10.1113/JP275328.
[34] A.S. Fanning, J.M. Anderson, Zonula occludens-1 and -2 are cytosolic scaffolds that regulate the assembly of cellular junctions, Ann. N. Y. Acad. Sci. 1165 (2009) 113–120, https://doi.org/10.1111/J.1749-6632.2009.04440.X.
[35] V.P. Orellana, A. Tittarelli, M.A. Retamal, Connexins in melanoma: potential role of Cx46 in its aggressiveness, Pigment. Cell Melanoma Res. 34 (5) (2021) 853–868, https://doi.org/10.1111/PCMR.12945.
[36] A. Tittarelli, I. Guerrero, F. Tempio, et al., Overexpression of connexin 43 reduces melanoma proliferative and metastatic capacity, Br. J. Cancer 113 (2) (2015) 259–267, https://doi.org/10.1038/BJC.2015.162.
[37] T. Aasen, M. Mesnil, C.C. Naus, P.D. Lampe, D.W. Laird, Gap junctions and cancer: communicating for 50 years, Nat. Rev. Cancer 16 (12) (2016) 775–788, https://doi.org/10.1038/NRC.2016.105.
[38] M. Ramirez Moreno, P.A. Stempor, N.A. Bulgakova, Interactions and feedbacks in E-cadherin transcriptional regulation, Front. Cell Dev. Biol. 9 (2021), https://doi.org/10.3389/FCELL.2021.701175.
[39] X. Tian, Z. Liu, B. Niu, et al., E-cadherin/β-catenin complex and the epithelial barrier, J. Biomed. Biotechnol. 2011 (2011), https://doi.org/10.1155/2011/567305.
[40] F.Z. Li, A.S. Dhillon, R.L. Anderson, G. McArthur, P.T. Ferrao, Phenotype switching in melanoma: implications for progression and therapy, Front. Oncol. 5 (FEB) (2015), https://doi.org/10.3389/FONC.2015.00031.
[41] H.G. Pálmer, M.J. Larriba, J.M. García, et al., The transcription factor SNAIL represses vitamin D receptor expression and responsiveness in human colon cancer, Nat. Med. 10 (9) (2004) 917–919, https://doi.org/10.1038/nm1095.
[42] E. Monaghan-Benson, K. Burridge, Mutant B-RAF regulates a Rac-dependent cadherin switch in melanoma, Oncogene 32 (40) (2013) 4836–4844, https://doi.org/10.1038/ONC.2012.492.
[43] P. Baquero, I. Sánchez-Hernández, E. Jiménez-Mora, J.L. Orgaz, B. Jiménez, A. Chiloeches, (V600E)BRAF promotes invasiveness of thyroid cancer cells by decreasing E-cadherin expression through a Snail-dependent mechanism, Cancer Lett. 335 (1) (2013) 232–241, https://doi.org/10.1016/J.CANLET.2013.02.033.
[44] S.R. Alonso, L. Tracey, P. Ortiz, et al., A high-throughput study in melanoma identifies epithelial-mesenchymal transition as a major determinant of metastasis, Cancer Res. 67 (7) (2007) 3450–3460, https://doi.org/10.1158/0008-5472.CAN-06-3481.
[45] E. Sánchez-Tilló, O. De Barrios, L. Siles, M. Cuatrecasas, A. Castells, A. Postigo, β-catenin/TCF4 complex induces the epithelial-to-mesenchymal transition (EMT)-activator ZEB1 to regulate tumor invasiveness, Proc. Natl. Acad. Sci. U. S. A. 108 (48) (2011) 19204–19209, https://doi.org/10.1073/PNAS.1108977108/-/DCSUPPLEMENTAL/PNAS.1108977108_SI.PDF.
[46] R.G. Hodge, A.J. Ridley, Regulating Rho GTPases and their regulators, Nat. Rev. Mol. Cell Biol. 17 (8) (2016) 496–510, https://doi.org/10.1038/nrm.2016.67, 2016;17(8).

Cerdido S. *et al* - Cancer Letters

Supplemental information

Supplemental Table 1. Sequences, protospacer adjacent motifs (PAM), efficiencies, and off-targets of the CRISPR plasmids used to stably knockdown MGRN1 expression in human melanoma cells.

sgRNA Oligo	Target sequence (5´→ 3´)	PAM	Score efficiency	Off-targets
sgRNA2	ATTCTCAGCCGCCGCATCGC	GGG	96.5	48
sgRNA3	CATCGACATCCAGGCGAACT	CGG	94.3	38
sgRNA4	GGACTTCGGAGGGTAGCGAT	AGG	91.7	49

Supplemental Table 2. Sequences of siRNA oligonucleotides used to deplete human MGRN1 and E-cadherin expression.

siRNA	Sequence
siGENOME Non-Targeting siRNA #2 (siCTR)	UAAGGCUAUGAAGAGAUAC
siGENOME Human MGRN1-1 (si-01)	CGAAGGAGAUGUGGUGGAA
siGENOME Human MGRN1-2 (si-02)	GAGCACCUUGUCCCUUUA
siGENOME Human MGRN1-3 (si-03)	GAACUCGGCCUAUCGCUAC
siGENOME Human MGRN1-4 (si-04)	AAGAUUGACUUCUCGGAAU
Universal Scrambled Negative Control siRNA Duplex (siCTR)	-
E-cadherin Human siRNA Oligo Duplexes -A (siA)	AGGCAAGGUUUUCUACAGCAUCACTG
E-cadherin Human siRNA Oligo Duplexes -B (siB)	CGUUUCUGGAAUCCAAGCAGAAUTG
E-cadherin Human siRNA Oligo Duplexes -C (siC)	GUCAGCUACUCUAGUUCUGUUGUTT

Supplemental Table 3. Sequences of forward and reverse primers used to amplify the specified target genes.

Target gene	Oligo sequence 5´ → 3´
CDH1	Forward: GACAGGATGCAGAAG Reverse: GCTCAGGAGGAGCAA
AXIN2	Forward: AGGGACAGGAATCATTCGGC Reverse: CACCTGCCAGTTTCTTTGGC
MITF	Forward: GGCAGACCTTGGTTTCCATA Reverse: ATGAGGAAATCTTGGGCTTGA
TCF7	Forward: GTTCACCCACCCATCCTTGA Reverse: TCTGCCTTGGACTCTGCTTG
cMYC	Forward: CACCACCAGCAGCGACTCT Reverse: GCCTGCCTCTTTTCCACAGA
LEF1	Forward: GAGAAAGGAGCAGGAGCCAA Reverse: TGCCACCTTCTGCCAAGAAT
ACTB	Forward: GGAAAGAGCGACCCTTACCA Reverse: AGGAGGAGACATAGGCGAGA

Supplemental Table 4. Sequences of the forward and reverse primers used for fragment-specific amplification and sequencing.

Target gene	Oligo sequence 5´ → 3´
NF1-PCR amplification	Forward: GATGAAAGTGCGCAAACAGG Reverse: CCATCTTATCAAAAGGTCGTC
NF1-Sequencing	Forward: TGATCGGTTTGAGAGAT Reverse: TGCATCACTTGTAGGACAATCAG

Supplemental Figure 1: Generation and validation of MGRN1-KO human melanoma cells. Related to Fig. 1.

A. Table showing genetic status of *NRAS*, *BRAF* (exon 15), *MC1R* and *NF1* (exons 27-33) in human melanoma cell lines (hMCs) HBL, MM28, DOR, BEU and C8161 and images of cellular pellets. **B.** Representative immunoblot (top) and quantification (bottom) of MGRN1 expression of hMCs. β-actin (Actin) was used as loading control. Intensity levels were normalized to HBL cells (n = 2, error bars are mean ±SEM). **C.** Quantification of the percentage of individual cells and cells forming collective aggregates upon MGRN1 knockdown in WT-BRAF melanoma cells (HBL, MM28 and DOR), after seeding the cells on collagen I (n = 2, error bars are mean ±SEM). **D.** Diagram depicting the targeted sequence of sgRNA2, sgRNA3 and sgRNA4 on exon 1 of *MGRN1* gene (underlined in blue). Pink line indicates the sequence of the protospacer adjacent motif (PAM). Red triangle points to the putative cleavage site of Cas9. **E.** Representative immunoblot of MGRN1 protein levels of MGRN1-null cells. β-actin (Actin) was used as loading control (error bars are mean ±SEM, n=2). **F.** Top: Edited sequence in exon 1 of *MGRN1* in MGRN1-KO clones 3.7 and 4.9, compared with the consensus sequence in control (CTR) HBL cells. Polymorphisms are highlighted in blue, deleted nucleotides are shown in red and inserted nucleotides are indicated in green. Bottom: amino acid sequence of the resulting truncated MGRN1 protein in MGRN1-KO cells.

A

Cell line	HBL	MM28	DOR	BEU	C8161
NRAS	WT/WT	WT/WT	Q61R/WT	WT/WT	WT/WT
BRAF exon 15	WT/WT	WT/WT	WT/WT	V600E/ V600E	V600E/ V600E
NF1 exons 27-33	WT/WT	WT/WT	WT/WT	WT/WT	WT/WT
MC1R	WT/WT	WT/WT	WT/WT	L93R/WT	R151C/WT
Phenotype		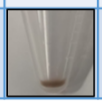		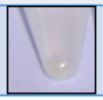	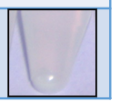

B

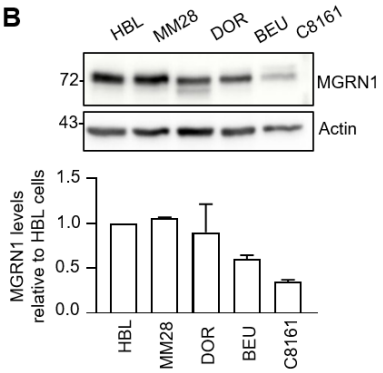

C

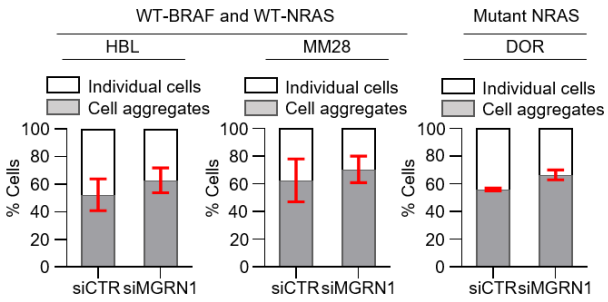

D

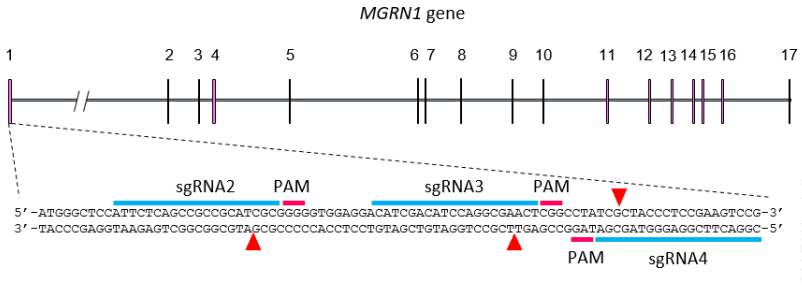

E

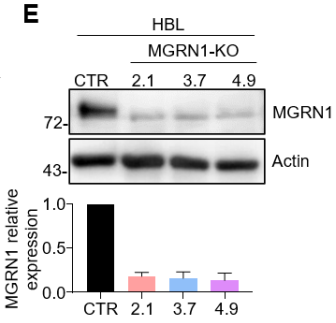

F

sgRNA clones	Edited sequences on *Mgrn1* exon 1
CTR	Alleles 1 and 2: ^{10}ATT CTC AGC CGC CGC ATC GCG GGG GTG GAG GAC ATC GAC ATC CAG GCG AAC TCG GCC TAT CGC TAC CCT CCG AAG TCC^{87}
3.7	Alleles 1 and 2: ^{10}ATT CTC AGC CGC CGC ATC GCG GGG TG GAG GAC ATC GAC ATC CAG GCG AAC TCG GCC TAT CGC TAC CCT CCG AAG TCC^{87}
4.9	Alleles 1 and 2: ^{10}ATT CTC ACC CGC CGC ATC GCG GGG GTG GAG GAC ATC GAC ATC CAG GCG AAC TCG GCC TAT CGGC TAC CCT CAG AAG TCC^{87}

Supplemental Figure 2: Analysis of cell adhesion molecules protein levels in MGRN1-null melanoma cells. Related to Fig. 3.

A. Representative immunoblots (top) and quantification (bottom) of N-cadherin (n = 3) and GJA1 (n = 4) in HBL MGRN1-KO cells. Protein levels were measured and referred to control cells (error bars are mean ±SEM). **B.** Representative confocal images (left) of ZO-1 (green) IF stainings and quantification of ZO-1 intensity levels (right) of HBL MGRN1-null cells. F-actin was also stained (red) and DAPI was used to stain DNA (blue). Scale bar 50 µm. Each dot represents a single cell. The graphs show the median of the relative intensity of ZO-1 relative to the cell area and normalized to control cells (n = 2 independent experiments, N = 47 cells, Kruskal Wallis test with Dunn's multiple comparisons was used to generate *P* value, ****$P < 0.0001$.

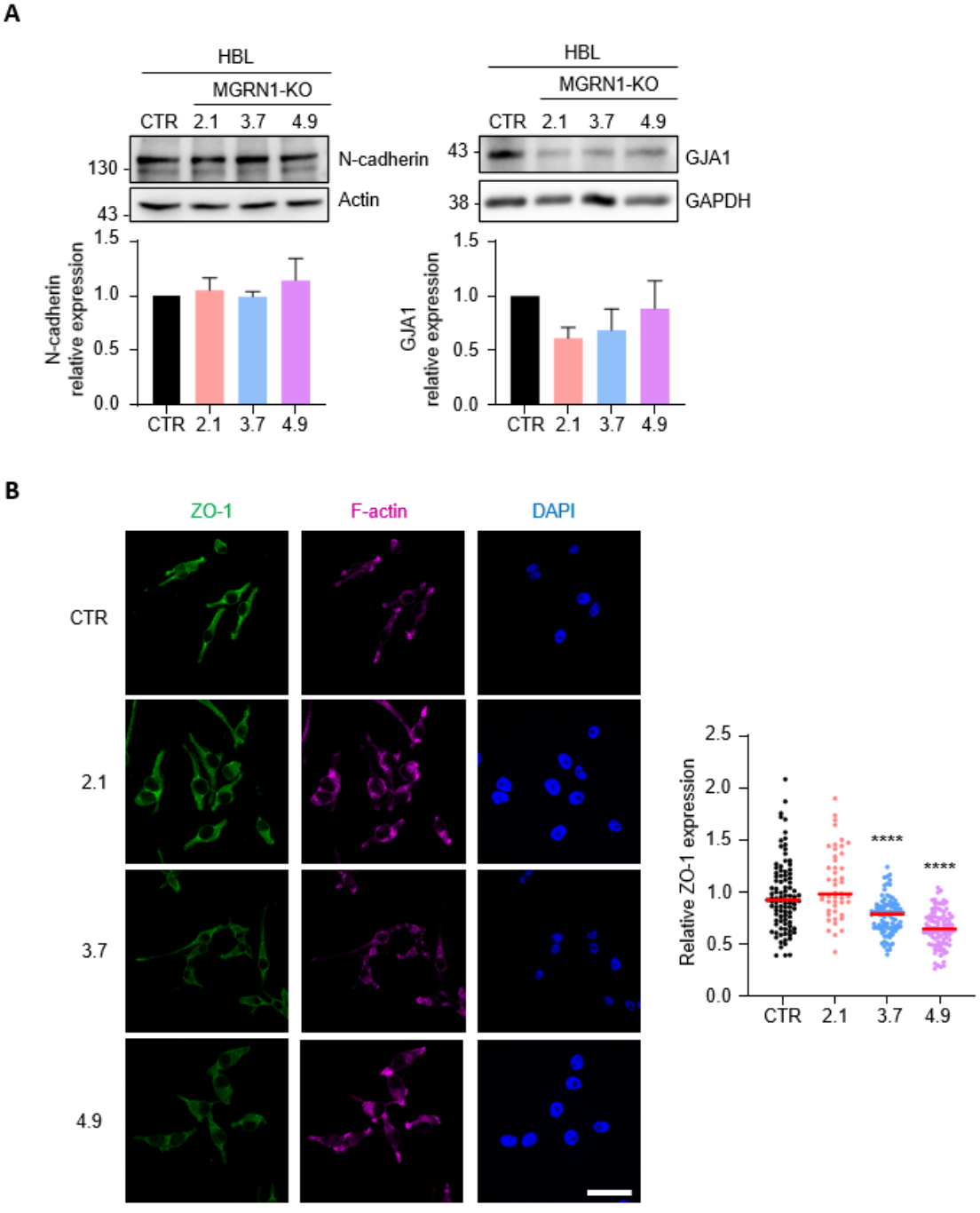

Supplemental Figure 3: Moderate reduction in β-catenin binding to chromatin in MGRN1-KO clones with no significant effect in canonical LEF1/β-catenin transcriptional activity. Related to Fig. 4.

A. Representative confocal images (left) of E-cadherin (green) and P-120 catenin (red) IF stainings using non-permeabilized nuclei conditions (0.1 % Saponin). F-actin was also stained (pink) and DAPI was used to stain DNA (blue). Scale bar 50 μm. The graphs show the median of intensity levels of P120 (top right) and co-localization (bottom right) between P-120 and E-cadherin using Manders' coefficient of HBL MGRN1-null cells compared with control cells. Each dot represents a single image (n = 2 independent experiments, N = 16 images, ANOVA test with Dunnett's multiple comparisons was used to generate *P* values, **P* < 0.05). **B.** Immunoblot (left) of β-catenin in HBL MGRN1-null cells after extraction of the chromatin-bound fraction in protein lysates using the CSK buffer. The transcription factor FOXM1 was used as nuclear marker and the glycolytic enzyme GAPDH as cytosolic protein. Chromatin-bound β-catenin intensity was normalized to chromatin-bound TATA-box Binding Protein (TBP). The graph on the right shows the quantification of the chromatin-bound β-catenin in MGRN1-KO cells (n = 4, error bars are mean ±SEM). **C.** Relative expression of *AXIN2* (n = 4)*, MITF* (n = 6)*, TCF7* (n = 4)*, cMYC* (n = 4)*,* and *LEF1* (n = 4) in control and MGRN1-KO cells estimated by qPCR (error bars are mean ±SEM).

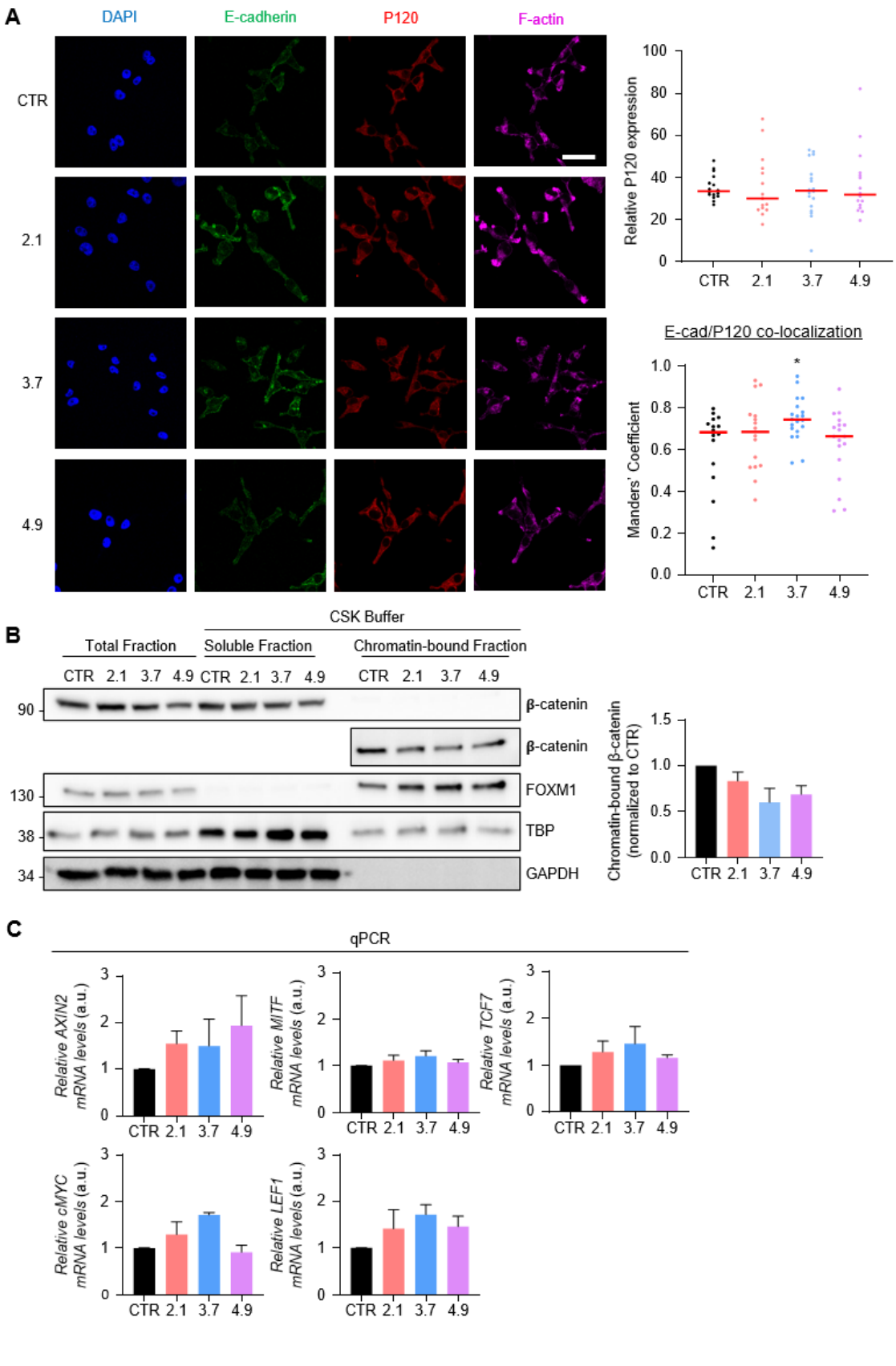
A
DAPI
E-cadherin
P120
F-actin
CTR
2.1
3.7
4.9
Relative P120 expression
100
80
60
40
20
0
CTR 2.1 3.7 4.9
E-cad/P120 co-localization
Manders' Coefficient
1.0
0.8
0.6
0.4
0.2
0.0
*
CTR 2.1 3.7 4.9
B
CSK Buffer
Total Fraction
Soluble Fraction
Chromatin-bound Fraction
CTR 2.1 3.7 4.9 CTR 2.1 3.7 4.9 CTR 2.1 3.7 4.9
90
β-catenin
β-catenin
130
FOXM1
38
TBP
34
GAPDH
Chromatin-bound β-catenin (normalized to CTR)
1.5
1.0
0.5
0.0
CTR 2.1 3.7 4.9
C
qPCR
Relative AXIN2 mRNA levels (a.u.)
Relative MITF mRNA levels (a.u.)
Relative TCF7 mRNA levels (a.u.)
Relative cMYC mRNA levels (a.u.)
Relative LEF1 mRNA levels (a.u.)
3
2
1
0
CTR 2.1 3.7 4.9

Supplemental Figure 4: E-cadherin depletion reverts the effect of decreased β-catenin nuclear localization upon MGRN1 knockdown. Related to Figure 6 and 7.

A. Immunoblot (top left) of E-cadherin after E-cadherin silencing for 48 h using siRNAs individually in HBL control and 2.1 clone cells. β-actin (Actin) was used as loading control. Phase-contrast images of MGRN1-KO melanoma cells (bottom left) seeded on a thick layer of collagen I in complete medium (scale bar 50 μm) and quantification of the area (bottom right) of the cellular clusters. Each dot represents a cellular aggregate and histogram shows the median of the area (n = 3 independent experiments, N = 145 cellular aggregates, *Mann-Whitney U* test was used to generate *P* values, **P* < 0.05, ***P* < 0.01, ***P < 0.001 and ****P<0.0001). **B.** Immunoblot (left) and quantification (right) of β-catenin protein levels after deletion of E-cadherin in MGRN1-KO cells. E-cadherin was detected to confirm effective knockdown and GAPDH as loading control. The graph shows β-catenin protein levels normalized to control cells (n = 2, error bars are mean ±SEM). **C.** Confocal images (left) and quantification (right) of β-catenin (green) of E-cadherin-silenced MGRN1-null cells. DAPI was used to stain DNA (blue). Scale bar 50 μm. Histogram shows quantification of the mean percentage of nuclear β-catenin. Each dot represents a single cell (n = 1, N = 50 cells, error bars mean ±SEM, *Welch´s t* test was used to generate *P* values, **P* < 0.05 and ****P < 0.0001). **D.** Immunoblots (left) and quantifications (right) of RAC-GAP1 (n=2) and ARH-GAP17 (n=4). β-Actin was used as loading control. Graphs show the mean ±SEM.

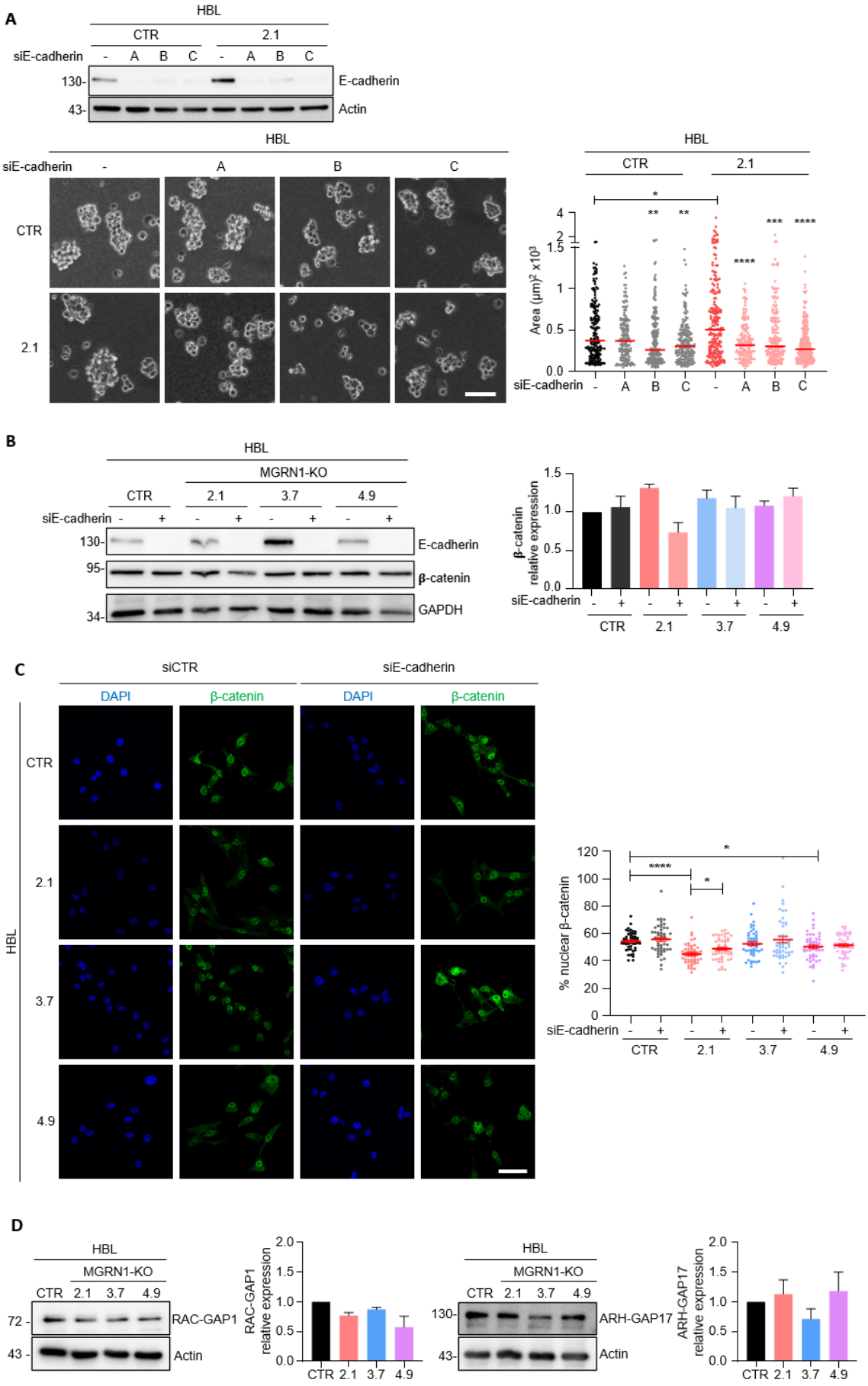
A
HBL
CTR
2.1
siE-cadherin - A B C - A B C
130-
E-cadherin
43-
Actin
HBL
siE-cadherin - A B C
CTR
2.1
HBL
CTR
2.1
Area (µm)² x10³
siE-cadherin - A B C - A B C
B
HBL
MGRN1-KO
CTR 2.1 3.7 4.9
siE-cadherin - + - + - + - +
130-
E-cadherin
95-
β-catenin
34-
GAPDH
β-catenin relative expression
siE-cadherin - + - + - + - +
CTR 2.1 3.7 4.9
C
siCTR
siE-cadherin
DAPI
β-catenin
DAPI
β-catenin
CTR
2.1
3.7
4.9
HBL
% nuclear β-catenin
siE-cadherin - + - + - + - +
CTR 2.1 3.7 4.9
D
HBL
MGRN1-KO
CTR 2.1 3.7 4.9
72-
RAC-GAP1
43-
Actin
RAC-GAP1 relative expression
CTR 2.1 3.7 4.9
HBL
MGRN1-KO
CTR 2.1 3.7 4.9
130-
ARH-GAP17
43-
Actin
ARH-GAP17 relative expression
CTR 2.1 3.7 4.9